



Published in final edited form as:

*Mol Cell*. 2020 March 05; 77(5): 951–969.e9. doi:10.1016/j.molcel.2019.12.028.

## AMPK, a key regulator of metabolism and autophagy, is activated by lysosomal damage via a novel galectin-directed ubiquitin signal transduction system

Jingyue Jia<sup>1,2,\*</sup>, Bhawana Bissa<sup>1,2,\*,#</sup>, Lukas Brecht<sup>3,\*</sup>, Lee Allers<sup>1,2</sup>, Seong Won Choi<sup>1,2</sup>, Yuexi Gu<sup>1,2</sup>, Mark Zbinden<sup>4</sup>, Mark R. Burge<sup>1,5</sup>, Graham Timmins<sup>1,6</sup>, Kenneth Hallows<sup>7</sup>, Christian Behrends<sup>3</sup>, Vojo Deretic<sup>1,2,\*\*,\*\*\*</sup>

<sup>1</sup>Autophagy, Inflammation and Metabolic Center of Biochemical Research Excellence, University of New Mexico Health Sciences Center, Albuquerque, NM, USA

<sup>2</sup>Department of Molecular Genetics and Microbiology, University of New Mexico School of Medicine, Albuquerque, NM, USA

<sup>3</sup>Munich Cluster of Systems Neurology, Ludwig-Maximilians-Universität München Feodor-Lynen Str. 17, 81377 München, Germany

<sup>4</sup>Human Metabolome Technologies America, Boston, MA, USA

<sup>5</sup>Department of Internal Medicine, University of New Mexico School of Medicine, Albuquerque, NM, USA

<sup>6</sup>School of Pharmacy, University of New Mexico Health Sciences Center, Albuquerque, NM, USA

<sup>7</sup>Division of Nephrology and Hypertension, Department of Medicine and USC/UKRO Kidney Research Center, Keck School of Medicine, University of Southern California, Los Angeles, CA, USA

### SUMMARY

AMPK is a central regulator of metabolism and autophagy. Here we show how lysosomal damage activates AMPK. This occurs via a hitherto unrecognized signal transduction system whereby cytoplasmic sentinel lectins detect membrane damage leading to ubiquitination responses.

Absence of Galectin 9 (Gal9) or loss of its capacity to recognize luminal glycans exposed during

\*\*Corresponding author.

#Bhawana Bissa's present address: Central University of Rajasthan, Ajmer, India

#### AUTHOR CONTRIBUTIONS

Conceptualization: J.J. B.B., V.D.; Investigation and Validation: B.B., L.B., J.J., Y.G., S.W.C.; Formal Analysis: B.B., J.J. C.B., G.T., M.B., K.H., V.D.; Resources: M.Z., K.H.; Data Curation: C.B., L.A.; Writing - Original Draft: V.D.; Writing - Review & Editing: J.J. C.B. M.B., G.T. K.H., V.D.; Visualization: L.A., B.B., J.J.; Supervision: C.B., V.D.; Project Administration: V.D.; Funding Acquisition: C.B., V.D.

\*Equally contributing authors

\*\*\*Lead contact

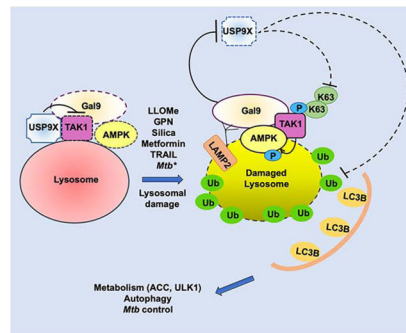
**Publisher's Disclaimer:** This is a PDF file of an unedited manuscript that has been accepted for publication. As a service to our customers we are providing this early version of the manuscript. The manuscript will undergo copyediting, typesetting, and review of the resulting proof before it is published in its final form. Please note that during the production process errors may be discovered which could affect the content, and all legal disclaimers that apply to the journal pertain.

#### DECLARATION OF INTERESTS

Mark Zbinden was an employee of Human Metabolome Technologies America, Boston, MA, USA.

lysosomal membrane damage abrogate such ubiquitination responses. Proteomic analyses with APEX2-Gal9 have revealed global changes within the Gal9 interactome during lysosomal damage. Gal9 association with lysosomal glycoproteins increases whereas interactions with a newly identified Gal9 partner, deubiquitinase USP9X, diminishes upon lysosomal injury. In response to damage, Gal9 displaces USP9X from complexes with TAK1 and promotes K63 ubiquitination of TAK1 thus activating AMPK on damaged lysosomes. This triggers autophagy and contributes to autophagic control of membrane-damaging microbe *Mycobacterium tuberculosis*. Thus, galectin and ubiquitin systems converge to activate AMPK and autophagy during endomembrane homeostasis.

## Graphical Abstract



## eTOC Blurb:

Jia, Bissa, Brecht et al., show that AMPK is activated upon lysosomal damage caused by microbes, ligands such as TRAIL, and other agents including the anti-diabetes drug metformin, via a novel signal transduction system from galectins to ubiquitin and that this results in the activation of AMPK by TAK1.

## INTRODUCTION

AMP-activated protein kinase (AMPK) is a ubiquitous metabolic regulator in eukaryotes (Hardie, 2014) acting as a cellular energy sensor and as a keeper of homeostatic levels of ATP (Herzig and Shaw, 2018; Lin and Hardie, 2018). Activation of AMPK results in inhibition of anabolic pathways consuming ATP and activation of catabolic pathways generating ATP, thus reprogramming cellular metabolism to restore energy balance (Hardie, 2014). The best known effects of AMPK are on intermediary metabolism (Hardie, 2014) and several global functions (Herzig and Shaw, 2018; Lin and Hardie, 2018) including autophagy (Egan et al., 2011; Garcia and Shaw, 2017; Herrero-Martin et al., 2009; Kim et al., 2013; Kim et al., 2011).

AMPK and its polar opposite, mTOR, which activates anabolic pathways (Saxton and Sabatini, 2017), have been implicated in diseases with metabolic perturbations (Garcia and Shaw, 2017) such as diabetes (He and Wondisford, 2015; Zhou et al., 2001) and cancer (Pineda et al., 2015). AMPK is also a modulator of the immune system, with immunometabolism being recognized as a determinant of immune responses (Gaber et al.,

2017; O'Neill et al., 2016). By opposing actions during immunometabolic switching, AMPK and mTOR influence innate and adaptive immunity (Gaber et al., 2017; O'Neill et al., 2016). AMPK (Egan et al., 2011; Garcia and Shaw, 2017; Herrero-Martin et al., 2009; Herzig and Shaw, 2018; Kim et al., 2013; Kim et al., 2011) and mTOR (Ganley et al., 2009; Hosokawa et al., 2009; Jung et al., 2009; Saxton and Sabatini, 2017) together control autophagy (Levine and Kroemer, 2019), a homeostatic process with roles in aging (Hansen et al., 2018; Madeo et al., 2019), obesity (Zhang et al., 2018), diabetes (Rivera et al., 2014), cancer (Kimmelman and White, 2017), immunity, inflammation, defense against intracellular pathogens (Deretic et al., 2013), and neurodegenerative diseases (Levine and Kroemer, 2019; Mizushima et al., 2008; Rubinsztein et al., 2015).

Autophagy plays a dual role as a metabolic process (Kimmelman and White, 2017; Kopitz et al., 1990; Rabinowitz and White, 2010) and as a cytoplasmic quality control (QC) pathway (Dikic and Elazar, 2018; Randow and Youle, 2014; Rogov et al., 2014). Its metabolic roles are manifested as starvation-induced turn-over of cytosolic proteins (Abu-Remaileh et al., 2017; Kopitz et al., 1990; Seglen et al., 1990), and degradation of ribosomes as cellular reservoirs of basic amino acids and nucleosides (An and Harper, 2018; Wyant et al., 2018). Autophagy mobilizes lipid (Dupont et al., 2014; Kopitz et al., 1990; Rambold et al., 2015; Seo et al., 2017; Settembre et al., 2013; Singh et al., 2009) and glycogen stores (Zirin et al., 2013). The QC functions of autophagy are manifested in selective removal of defunct organelles such as mitochondria (Lazarou et al., 2015), ER (Khaminets et al., 2015), peroxisomes (Marcassa et al., 2018), protein aggregates (Bjorkoy et al., 2005; Dikic and Elazar, 2018; Rogov et al., 2014) and damaged lysosomes (Maejima et al., 2013). Autophagy's action in innate defense against invading microbes, falls under the rubric of cytoplasmic QC (Deretic et al., 2013).

Lysosomal damage strongly activates autophagy exceeding starvation as a benchmark inducer (Chauhan et al., 2016; Jia et al., 2018). Autophagy removes damaged lysosomes (Maejima et al., 2013) once they are beyond repair (Radulovic et al., 2018; Skowyra et al., 2018). The complexity of the relationship between autophagy and lysosomes is that autophagosomal and endolysosomal organelles merge during the final steps of autophagy so that the sequestered autophagic cargo can be digested in autolysosomes or otherwise eliminated (Levine and Kroemer, 2019). Thus, lysosomal homeostasis (Radulovic et al., 2018; Skowyra et al., 2018), including their reformation (Yu et al., 2010) and de novo biogenesis (Sardiello et al., 2009; Settembre et al., 2011) is of a paramount importance for functional autophagy. Hence, countering lysosomal injury, via membrane repair (Radulovic et al., 2018; Skowyra et al., 2018) or elimination of damaged lysosomes (lysophagy) (Maejima et al., 2013) coupled with their replacement through biogenesis (Sardiello et al., 2009; Settembre et al., 2011), is necessary for cellular fitness. Lysosome damage occurs physiologically, e.g. during exposure to exogenous and endogenous agents including biologically active crystals of silica, monosodium urate, and cholesterol (Maejima et al., 2013; Razani et al., 2012; Schroder and Tschopp, 2010), proteopathic fibrils or amyloid (Heneka et al., 2013; Masters et al., 2010; Papadopoulos et al., 2017; Parry et al., 2015), and microbial invasion involving directly or indirectly lysosomal compartments (Fujita et al., 2013; Jia et al., 2018; Maejima et al., 2013).

AMPK can be activated by different stressors that alter cellular energy levels including glucose starvation, hypoxia, ischemia, and oxidative damage (Hardie, 2011; Herzig and Shaw, 2018; Lin and Hardie, 2018). In the majority of these processes, AMPK subunits react to reduced cellular energy charge (e.g. increased AMP:ATP ratios). However, AMPK can be activated by nucleotide-independent mechanisms (Lin and Hardie, 2018) whereby the absence of a specific glycolytic intermediate, fructose 1,6 bisphosphate (FBP), triggers AMPK activation on lysosomes (Li et al., 2019; Zhang et al., 2017). Whether other signals activating AMPK utilize this new or other yet to be uncovered pathways is not known. There are three upstream kinases, LKB1 (Woods et al., 2003), CAMKK2 (Hawley et al., 2005) and TAK1 (Momcilovic et al., 2006) that can activate AMPK by phosphorylation at T172. LKB1 is considered to be the dominant AMPK kinase (Hardie, 2014; Herzig and Shaw, 2018; Lin and Hardie, 2018). CAMKK2 is a well-accepted alternative AMPK kinase (Herzig and Shaw, 2018). TAK1 is a less prominent T172 kinase of AMPK still in a search of its true physiological role in AMPK activation (Neumann, 2018). Importantly, activation of TAK1 does not always lead to AMPK activation (Herrero-Martin et al., 2009), and whether AMPK is activated by TAK1 depends on the context. At present, unifying physiological circumstances for AMPK activation by TAK1 remain elusive (Neumann, 2018).

AMPK is activated by lysosomal damage, but the mechanism has not been elucidated (Jia et al., 2018). During lysosomal damage two independent systems spring into action - galectins and ubiquitin. Galectins are a family of cytosolic lectins recognizing  $\beta$ -galactoside glycans, with less understood intracellular functions and primarily being appreciated for their extracellular signaling (Johannes et al., 2018). Ubiquitin has been well studied during selective autophagy as it opsonizes cargo for autophagic receptors (Kirkin et al., 2009). Ubiquitination also controls stability of several autophagy regulators (Liu et al., 2016; Nazio et al., 2013). Ubiquitin remodeling on lysosomes by VCP/p97 is needed for efficient lysophagy (Papadopoulos et al., 2017). During lysophagy, galectin and ubiquitin responses are considered to act as “eat me” signals recruiting autophagy receptors and autophagy machinery (Chauhan et al., 2016; Maejima et al., 2013; Papadopoulos et al., 2017). In this context, the best example is the autophagic receptor NDP52 which binds both Galectin 8 (Gal8) and ubiquitin (Thurston et al., 2012). A recent study showing that cytoplasmic Gal8 inhibits mTOR during lysosomal damage (Jia et al., 2018), suggests that intracellular galectins may play wider regulatory roles. However, that is yet to be broadly investigated. Furthermore, any functional interplays between galectins and ubiquitination responses have not been addressed beyond an assumption that they act as additive opsonization signals for selective autophagy.

Here we show how AMPK is activated in response to lysosomal damage and that galectins and ubiquitin play regulatory and cooperative roles in AMPK activation leading up to autophagy induction. This cascade starts by the recognition of membrane damage by galectins, specifically by Gal9. Unexpectedly, we found that Gal9 was necessary for efficient ubiquitination during lysosomal damage. Thus, we uncovered a signal transduction pathway between the membrane integrity sentinel lectins and the ubiquitin system.

## RESULTS

### Lysosomal damage-induced ubiquitination depends on Gal9

Lysosomal damage activates mTOR and inactivates AMPK (Jia et al., 2018). Both mTOR and AMPK are master regulators of cellular metabolism (Garcia and Shaw, 2017; Hardie, 2011; Herzig and Shaw, 2018; Lin and Hardie, 2018; Saxton and Sabatini, 2017). In keeping with this, lysosomal damage affected metabolism as indicated by metabolomic analyses (Table S1, Tab1). Here, we focused on the mechanism of how lysosomal damage activated AMPK. Lysosomal membrane damage induces both galectin and ubiquitin responses (Aits et al., 2015; Chauhan et al., 2016; Maejima et al., 2013; Papadopoulos et al., 2017). We wondered whether they may be connected. There are three major galectin responders, Galectin 3 (Gal3), Gal8 and Gal9, to endolysosomal (Aits et al., 2015; Chauhan et al., 2016; Jia et al., 2018; Maejima et al., 2013) and phagosomal damage (Dupont et al., 2009; Fujita et al., 2013; Garin et al., 2001; Paz et al., 2010; Thurston et al., 2012). Gal3, Gal8 and Gal9 form puncta on lysosomes damaged by agents such as Leu-Leu-OMe (LLOMe) (Aits et al., 2015; Jia et al., 2018; Thiele and Lipsky, 1990), glycyl-L-phenylalanine 2-naphththylamide (GPN) (Berg et al., 1994) and silica (Jia et al., 2018; Maejima et al., 2013). Huh7 liver adenocarcinoma cells consistently express all three responder galectins, Gal3, Gal8, and Gal9. We tested whether their knockdowns affected ubiquitination responses in Huh7 cells treated with LLOMe. No effect was observed with Gal3 and Gal8 but Gal9 knockdown reduced the ubiquitin response quantified by high content microscopy (HCM) (Figs. 1A and S1A). We confirmed these relationships in primary human peripheral blood monocyte-derived macrophages (Figs. S1B and S1C). CRISPR Gal9 knockout in Huh7 cells (Gal9KO<sup>Huh7</sup>) (Figs. 1B, C and S1D) showed diminished, albeit not completely abrogated, ubiquitin puncta response to LLOMe (Figs. 1B and 1C). Ubiquitin puncta were on lysosomes, and reduced ubiquitination of lysosomes was observed in Gal9KO<sup>Huh7</sup> cells (Fig. 1D). Reduced protein ubiquitination in response to lysosomal damage was detected in cell lysates (Fig. S1E) and in lysosomal preparations purified from Gal9KO<sup>Huh7</sup> cells by LysoIP (Abu-Remaileh et al., 2017). In LysoIP, TMEM192–3xHA transfected cells are used to immunopurify lysosomal organelles on anti-HA beads, and, in parallel, TMEM192–2xFLAG transfected cells are used as a control for specificity of immunoisolation on anti-HA beads (Fig. S1F). Thus, Gal9 is required for the ubiquitination response during lysosomal damage (Fig. 1E).

### Proteomic proximity analysis of Gal9 during lysosomal damage

We next investigated partners of Gal9 for clues regarding how Gal9 control ubiquitination response to lysosomal damage. We generated a stable cell line expressing APEX2-myc-Gal9 in HEK293T (APEX2-Gal9–293T<sup>stable</sup>) cells and subjected them to lysosomal damage with LLOMe (Fig. 1F). Consistent with a role for Gal9 in the ubiquitination response to lysosomal damage, APEX2-Gal9–293T<sup>stable</sup> cells showed a robust ubiquitination response to LLOMe treatment in immunoblots relative to HEK293T cells, which normally display only low levels of endogenous Gal9 (Figs. S1G and S1H). APEX2-Gal9–293T<sup>stable</sup> cells were subjected to differential SILAC labeling, proximity biotinylation in conjunction with LLOMe treatment, and biotinylated proteins analyzed by LC-MS/MS. Volcano plots of SILAC LC-MS/MS results quantifying alterations in proximity of cellular proteins to

APEX2-Gal9 (Fig. 1G) revealed dynamic changes upon lysosomal damage. Gal9 interaction candidates belonged to several discernible functional groups: (i) integral lysosomal membrane proteins (e.g. LAMP1, LAMP2, SCARB/LIMP-2, VAMP7, TMEM192; showing increased association); (ii) lysosomal and other lipid metabolism proteins (NPC1, CDIPT-PIS, HSD17B10; increased association); (iii) ubiquitin transactions proteins (TRIM25, VCP, USP7 and USP9X; damage-neutral or decreased association); (iv) ESCRT or ESCRT-related proteins (TSG101, PDCD6IP-ALIX, SRI; decreased or damage-neutral association); (v) TORC1 regulators and mTOR effectors (LAMTOR1, EIF3L; increased or decreased associations); and (vi) a group of diverse partners (SYNCRIP, IMPDH2, EZR, JUP-catenin, ACTN4-actinin, SEC24B or C; primarily reduced associations).

APEX2-Gal9 showed proximity to integral membrane lysosomal proteins LAMP1, LAMP2, and TMEM192, as well as the SNARE protein VAMP7, all previously shown to be targeted by FBXO27, a glycan-recognizing component of the SCF (SKP1-CUL1-F-box protein) ubiquitin ligase complex (Yoshida et al., 2017), consistent with Gal9 translocation to lysosomes after damage (Aits et al., 2015; Jia et al., 2018; Thurston et al., 2012).

### Gal9 recruitment to damaged lysosomes regulates ubiquitination response

We confirmed interactions of LAMP1 and LAMP2 with Gal9 employing APEX2-Gal9–293T<sup>stable</sup> cells for BioWeB analysis (proximity biotinylation combined with affinity enrichment on avidin beads and Western blotting) (Figs. S2A and 2A) and by co-IP between GFP-Gal9 and endogenous LAMP2 (Fig. S2B). The interaction was specific for Gal9, as Gal8 did not co-IP with LAMP2 when compared to Gal9 (Fig. S2B). The Gal9-LAMP2 interaction required Gal9's ability to recognize glycans exposed on damaged lysosomal membranes. When we mutated R65 and R239 in the carbohydrate recognition domains 1 and 2 (CRD1 and CRD2) previously shown to abrogate Gal9's ability to bind  $\beta$ -galactoside glycoconjugates (Matsushita et al., 2000; Zhu et al., 2005), the association between mutant Gal9 and LAMP2 was lost (Fig. 2B).

We generated an inducible (Tet-ON) stable cell line using the FLP-FRT recombination system (HeLa Flp-In Gal9<sup>Tet-ON</sup>), and detected time-dependent (during LLOMe treatment) Gal9 puncta formation as early as at 10 min with a plateau at 30–60 min (quantified by HCM; Fig. S2C). The mCherry-Gal9 puncta overlapped with LAMP2, as quantified by HCM (Fig. S2D) and observed by confocal microscopy (Fig. S2E). The mCherry-Gal9 puncta overlapped with ubiquitin dots elicited by LLOMe (Fig. S2F). There was colocalization of the three markers (mCherry-Gal9, LAMP1 and ubiquitin) (Fig. S2G). To test whether Gal9-puncta depended on glycan recognition, we compared FLAG-Gal9<sup>WT</sup> transfected-cells with FLAG-Gal9<sup>R65A/R239A</sup>, FLAG-Gal9<sup>R65A</sup> and FLAG-Gal9<sup>R239A</sup> mutants and found that glycan-binding mutants lost the ability to form puncta upon lysosomal damage (Figs. 2C and S2H) as quantified by HCM (Fig. 2D).

The Gal9 glycosylation mutants were tested in complementation experiments. The ubiquitination response was assessed by immunoblotting after 30 min incubation with LLOMe as in Fig. S1E; complementation of Gal9KO<sup>Huh7</sup> cells was achieved only with FLAG-Gal9<sup>WT</sup> and not with FLAG-Gal9<sup>R65A</sup>, FLAG-Gal9<sup>R239A</sup>, or FLAG-Gal9<sup>R65A/R239A</sup> (Fig. S2I). In imaging experiments, FLAG-Gal9<sup>R65A/R239A</sup> mutant did not rescue ubiquitin

puncta in response to lysosomal damage in Gal9KO<sup>Huh7</sup> cells whereas FLAG-Gal9<sup>WT</sup> did, as detected by confocal microscopy (Fig. 2E) and quantified by HCM (Fig. 2F).

Thus, Gal9 is recruited to damaged lysosomes where it interacts with lysosomal glycoproteins including LAMPs (Fig. 2G) and recognition of exposed glycans by Gal9 CRDs is important for the role of Gal9 in the ubiquitination response to lysosomal damage.

### Deubiquitinating enzyme USP9X is a Gal9 effector in ubiquitin response to lysosomal damage

The lack of FBXO27 and other components of the SCF E3 ligase among Gal9 interactors suggests that Gal9 may employ a different mechanism than a reported recruitment of SCF<sup>FBXO27</sup> (Yoshida et al., 2017). An additional proteomic proximity biotinylation analysis with APEX2-Gal9-293T<sup>stable</sup> cells was carried out using a different agent, GPN, titrated to cause only mild lysosomal damage (Fig. 3A). Albeit several differences were observed with GPN, a number of entities from the protein groups observed with LLOMe were found in the proximity of Gal9. This included: TSG101 and SRI of the ESCRT group, implicated in lysosomal damage repair (Skowyra et al., 2018); integral lysosomal proteins LAMP1 and LAMP2; ubiquitin transactions proteins including deubiquitinases (DUBs) USP7 (Pozhidaeva and Bezsonova, 2019) and USP9X (Paudel et al., 2019; Schwickart et al., 2010); a ubiquitin E3 ligase TRIM25 (Gack et al., 2007); and VCP, a part of the ELDR complex (p97-UBXD1-PLAA-YOD1) involved in remodeling of K48 ubiquitin chains on damaged lysosomes (Papadopoulos et al., 2017). As with LLOMe, FBXO27 or components of the SCF E3 ubiquitin ligase (Yoshida et al., 2017) were not among Gal9 interactors using GPN. TRIM25 was seen in proteomic analyses with both LLOMe and GPN but did not show a change during lysosomal damage. VCP removes K48 ubiquitin from lysosomal substrates as a prelude to other events (Arhzaouy et al., 2019). However, we did not find other components of the ELDR complex. We next focused on the DUBs identified in both LLOMe and GPN proteomic analyses. Of the two (USP7 and UPS9X), USP9X peptide counts were higher vs. USP7 and Log2 fold change for USP9X was greater in both LLOMe and GPN experiments whereas the p value for the change showed greater statistical significance (volcano plots in Fig. 1G and 3A and Table S1, Tabs 2–4). Thus we focused in subsequent experiments on USP9X, previously implicated in stabilization of a number of important substrates including Beclin 1 (Elgendy et al., 2014; Li et al., 2018) and AMPK-related kinases (Al-Hakim et al., 2008).

We confirmed Gal9 and USP9X interactions and examined their dynamics during lysosomal damage. FLAG-Gal9 and USP9X interacted in resting cells by co-IP (Fig. 3B). We mapped the interaction domain in Gal9 to its CRD2 (Figs. S3A and S3B). Interactions between FLAG-Gal9 and USP9X decreased upon LLOMe treatment (Fig. 3B), in keeping with the dynamic proximity biotinylation proteomic analyses with LLOMe (Fig. 1G) or GPN (Fig. 3A). USP9X did not form puncta either in resting or cells exposed to LLOMe (Fig. S3C). Gal9-USP9X interactions in resting cells were independent of Gal9's capacity to recognize glycans (Fig. 3C). Hence, Gal9 and USP9X interact primarily under homeostatic conditions. However, USP9X dissociated from Gal9 complexes during damage, and this depended on the ability of Gal9 to recognize exposed glycans (Fig. 3C), indicating that recognition of

lysosomal membrane damage by Gal9 acts as a signal prompting separation of Gal9 and USP9X. Thus, USP9X is a Gal9 interacting partner responsive to lysosomal damage (Fig. 3I).

We tested the role of USP9X in ubiquitin response. In Gal9KO<sup>Huh7</sup> cells, knocking down USP9X reversed the loss of ubiquitin puncta during lysosomal damage (Figs. 3D–F and S3E). The restored ubiquitin puncta overlapped with LAMP1 (Fig. S3D). In WT Huh7 cells, a USP9X knockdown did not have these effects (Fig. 3D). We overexpressed FLAG-USP9X in Huh7 cells (WT and Gal9<sup>KO</sup>), and quantified overlaps between USP9X and lysosomes (LAMP1) by HCM in cells subjected to damage. After 30 min of LLOMe treatment, WT cells showed reduced FLAG-USP9X association with lysosomes, whereas in Gal9KO<sup>Huh7</sup> cells the lysosomal localization of FLAG-USP9X did not diminish (Fig. 3G). In experiments with LysoIP, the cells expressing FLAG-USP9X had FLAG-USP9X on lysosomes under resting conditions (no LLOMe). However, FLAG-USP9X was fully removed from lysosomes upon LLOMe treatment (Fig. 3H). The departure of FLAG-USP9X from lysosomes was ineffective in Gal9KO<sup>Huh7</sup> cells (Fig. 3H). Thus, in the absence of Gal9, USP9X acts to remove ubiquitin, but when Gal9 is present and can recognize membrane injury, Gal9 excludes USP9X and promotes the ubiquitination response (Fig. 3I).

### Roles of Gal9, USP9X, and ubiquitin converge upon TAK1, a regulator of AMPK

Our recent studies found Gal9 in complexes with AMPK and one of its upstream activating kinases, TAK1, but whether these complexes respond to lysosomal damage is not known (Jia et al., 2018). We detected by BioWeB assay increased association between AMPK and Gal9 at 30 min of exposure to LLOMe (Fig. S4A). A similar increase in mCherry-Gal9 association with GFP-TAK1 was observed at 30 min of LLOMe treatment in HeLa Flp-In Gal9<sup>Tet-ON</sup> cells (Fig. S4B). Gal9 is important for ubiquitination (see above) whereas TAK1 is activated by K63 ubiquitination (Fan et al., 2010; Yang et al., 2015). TAK1 was ubiquitinated upon lysosomal damage, detected in IPs of FLAG-TAK1 coexpressed with HA-tagged ubiquitin (Fig. 4A). Gal9 was critical for TAK1 ubiquitination, as evident by comparing Gal9KO<sup>Huh7</sup> vs WT Huh7 cells (Fig. 4A). When Gal9 was overexpressed in HEK293T cells, which have low levels of endogenous Gal9, this increased TAK1 ubiquitination, correlating with detection of Gal9 in protein complexes with GFP-TAK1 (Fig. 4B). The Gal9 mutants that cannot translocate to damaged lysosomes (Figs. 2C and 2D) could not rescue ubiquitination defect in Gal9KO<sup>Huh7</sup> (Figs. 2E and 2F). When overexpressed in HEK293T cells, FLAG-Gal9<sup>R65A</sup>, FLAG-Gal9<sup>239A</sup> and FLAG-Gal9<sup>R65A/R239A</sup> did not support TAK1 ubiquitination in LLOMe-treated cells, whereas FLAG-Gal9<sup>WT</sup> did (Fig. 4C).

The endogenous USP9X DUB was detected in complexes with TAK1 using FLAG-TAK1-expressing 293T cells (Fig. 4D). Dissociation of USP9X and TAK1 upon LLOMe-treatment depended on Gal9, evidenced by increased USP9X in complexes with FLAG-TAK1 in Gal9KO<sup>Huh7</sup> cells (Fig. 4E). Cells expressing escalating levels of Gal9 displayed decreasing TAK1-USP9X associations (Fig. 4D). This corresponded to increased K63 ubiquitination of TAK1 (Fig. 4D). We tested whether ubiquitination of TAK1 enhanced by Gal9 was K48 or K63 linked. For that, we co-expressed GFP-Gal9 with either HA-Ub-K63 (all K residues

mutated to R except K63), HA-Ub-K48 (all K residues mutated to R except K48), or HA-Ub-WT, and observed enhanced ubiquitination of TAK1 with WT and K63 ubiquitin but not with K48 ubiquitin (Fig. S4C). The Gal9-induced dissociation of TAK1 and USP9X was detected in these experiments (Fig. S4C). TAK1 activation, monitored by T184 phosphorylation (Liu et al., 2018; Yu et al., 2008), increased upon lysosomal damage in Huh7 WT cells but showed a reverse trend in Gal9KO<sup>Huh7</sup> (Fig. 4F). Knocking down USP9X in Gal9KO<sup>Huh7</sup> cells rescued TAK1 activation, reflected in its K63 ubiquitination (Fig. S4D) and pT184 phosphorylation (Fig. 4G). Thus, by interfering with USP9X, Gal9 is important for TAK1 K63 ubiquitination and activation (Li et al., 2011; Wang et al., 2001) in response to lysosomal damage.

### AMPK activation during lysosomal damage depends on TAK1

AMPK was activated in a time-dose dependent manner and by diverse damaging agents (LLOMe, GPN, and silica) (Figs. S4E–F) as reflected in AMPK targets, ACC (pS79) (Figs. S4E–F) and ULK1 (pS555) (Fig. S4E), including the upstream kinase TAK1 in HeLa cells (Fig. S4G). TAK1 has been identified in Gal9 complexes (Jia et al., 2018). We tested whether this was affected by lysosomal damage using the BioWeB assay and a stable cell line expressing APEX2-AMPK $\alpha$ 1 subunit in 293T cells (Flp-In APEX2-AMPK $\alpha$ 1<sup>Tet-ON</sup>; Fig. 5A). TAK1, but not LKB1 or CaMKK2, was in proximity of AMPK $\alpha$ 1 in cells subjected to lysosomal damage (Fig. 5B). We next tested different inducing conditions (Fig. 5C). LKB1 was in proximity of APEX2-AMPK $\alpha$ 1 in cells treated with oligomycin A, a mitochondrial ATP synthase inhibitor, and so was the LKB1 adaptor/scaffold factor Axin (Li et al., 2019; Zhang et al., 2017; Zhang et al., 2014; Zhang et al., 2013) during glucose starvation (Fig. 5C). CaMKK2 associated with APEX2-AMPK $\alpha$ 1 only in cells treated with Ca<sup>2+</sup> ionophores ionomycin or A23187 (Fig. 5C). TAK1 associated with APEX2-AMPK $\alpha$ 1 during lysosomal damage exclusively and some LKB1 associated with APEX2-AMPK $\alpha$ 1 under prolonged lysosomal damage (Fig. 5C).

Treatment of Huh7 cells with TAK1 inhibitor resorcylic lactone 5ZO ((5-Z)-7-oxozeaenol) (Okada et al., 2014; Wu et al., 2013) prevented AMPK $\alpha$ 1 activation by lysosomal damage (Fig. 5D). In Huh7 cells, LKB1 was sequestered in the nucleus and did not translocate to the cytoplasm on LLOMe treatment, although it did with glucose starvation (Fig. S4H). 5ZO suppressed TAK1 activation by LLOMe in HeLa cells, a cell line notorious for downregulation or absence of LKB1 (McCabe et al., 2010) (Fig. 5D), and phosphorylation of AMPK $\alpha$ 1 (pT172) and its substrate ACC (pS79). In addition to using TAK1 enzymatic inhibitors, we employed MEFs lacking TAB2, an upstream ubiquitin-chain binding activator of TAK1 (Criollo et al., 2011; Takaesu et al., 2012), and detected no increase in p172 AMPK $\alpha$ 1 and pS79 ACC, although the matching WT TAB2 MEFs responded to lysosomal damage (Fig. 5E). In complementary experiments, we used TRAIL as a known agonist of AMPK activation via TAK1 (Herrero-Martin et al., 2009). A responder cell line, THP-1, displayed AMPK $\alpha$  phosphorylation after 1 h of TRAIL treatment (Fig. 5F). TRAIL induces lysosomal permeabilization (Werneburg et al., 2007), and thus we tested whether we could detect Gal9 and ubiquitin puncta. THP-1 cells displayed increased Gal9 and ubiquitin puncta upon stimulation with TRAIL (Figs. 5G and

5H). The ubiquitin response to TRAIL was reduced in cells knocked down for Gal9 (Fig. 5H).

LKB1 can contribute to AMPK activation in response to prolonged lysosomal damage (Jia et al., 2018). We knocked down LKB1, TAK1, and CaMKK2 in Huh7 cells, tested AMPK activation at early time point (30 min of damage), and observed that AMPK activation is independent of LKB1 and CaMMK2 at that time point but fully dependent on TAK1 (Fig. 5I). As expected, at later time points of LLOMe treatment, AMPK activation needed both TAK1 and LKB1 while still remaining independent of CaMMK2 (Fig. 5J). This correlated with changes in AMP/ATP ratios, which were not altered during the first 30 min of LLOMe treatment but increased at later time points (Fig. 5K). LKB1 translocation from the nucleus was observed with longer LLOMe treatment (Fig. S4I), coinciding with detection of LKB1's contribution to AMPK activation. Thus, TAK1 is the kinase activating AMPK in response to the lysosomal damage (acting solo during the early stages) and later, with sustained damage when AMP/ATP ratios increase, LKB1 joins TAK1 in the overall activation of AMPK.

### Activated AMPK translocates to lysosomes in a Gal9-dependent manner

AMPK $\alpha$  was detected by immunoblotting on lysosomes purified by LysoIP (Figs. S1F and 6A,B). AMPK enrichment on membranes was detected in 100k pellets positive for LAMP2 (Fig. S5A). AMPK detected by LysoIP was in activated state (pT172-AMPK $\alpha$ 1; Fig. 6C). By LC-MS/MS quantitative DIA analysis of LysoIP-purified lysosomes (Fig. 6A), there was a 32-fold median enrichment of TAK1, a twofold increase of TAB1, and a 10-fold enrichment of TAB2 on lysosomes upon LLOMe damage (30 min), contrasted by a twofold decrease in USP9X (Fig. 6D and Table S1, Tabs 7–9).

AMPK translocation to damaged lysosomes depended on Gal9, because there was less enrichment of AMPK $\alpha$ 1 on lysosomes in Gal9KO<sup>Huh7</sup> than in their parental Huh7 Gal9 WT cells (Figs. 6A,E). AMPK activation and phosphorylation of ACC depended on Gal9 (comparing Gal9KO<sup>Huh7</sup> and parental Gal9WT<sup>Huh7</sup> cells) (Fig. 6F). The absence of AMPK and ACC activation in Gal9KO<sup>Huh7</sup> was reversed by USP9X knockdown (Fig. 6G). Thus, Gal9 helps activate AMPK and recruits it to lysosomes following damage whereas the DUB USP9X antagonizes AMPK activation (Fig. 6H).

### Metformin causes lysosomal damage

Metformin, an AMPK inducer, is a widely used antidiabetic drug (Foretz et al., 2014). However, its precise mode of action remains unclear (He and Wondisford, 2015). Recent studies (Zhang et al., 2016) have shown that metformin can induce AMPK through a lysosomal pathway involving AXIN and LKB1. We thus wondered whether metformin may affect lysosomal membrane integrity. Effects of metformin on cells are highly dependent on its transport and high concentrations are used experimentally (He and Wondisford, 2015) including 2 mM for 12 h (Zhang et al., 2016). We used a macrophage cell line THP-1 (Huh7 or 293T cells did not respond) with 250  $\mu$ M metformin for 2 h and observed a lysosomal damage response by Gal9 puncta formation (Fig. S5B) and an increase in Gal8 puncta, another galectin responding to lysosomal damage (Aits et al., 2015; Jia et al., 2018) (Fig. S5B). We also observed a mild ubiquitination response (Fig. S5C). Gal9 and ubiquitin

response was detected in Huh7 cells treated with 250  $\mu$ M metformin only when they were transfected with organic cation transporter OCT1 (He and Wondisford, 2015) (SLC22A1; Figs. S5D and S5E). 293T cells do not express sufficient levels of endogenous Gal9 (Fig. S1H) to permit similar analyses. Nevertheless, APEX2-Gal9-293T<sup>stable</sup> cells transfected with SLC22A1 displayed a ubiquitination response to 250  $\mu$ M metformin treatment for 2 h detected by immunoblotting (Fig. S5F).

Evidence of lysosomal damage was detected by decreased staining with the acidotropic dye LysoTracker Red, which is normally trapped in acidified compartments such as lysosomes (Fig. S5G). Furthermore, the number of puncta positive for MagicRed, a fluorescent reporter for lysosomal cathepsin B activity, was reduced (Fig. S5H). ALIX, an ESCRT marker of lysosomal membrane damage repair (Radulovic et al., 2018; Skowyra et al., 2018) showed a response to metformin (Fig. S5I). We conclude that metformin is capable of causing lysosomal damage, a process that activates AMPK.

### Gal9 and USP9X regulate autophagy induction in response to lysosomal damage

LLOMe has been shown to induce autophagy (Aits et al., 2015; Chauhan et al., 2016; Jia et al., 2018; Maejima et al., 2013; Thurston et al., 2012). We observed a similar LC3 response to metformin (Fig. 7A), in a dose response dependent manner (Fig. 7B). Lysosomal damage inhibits mTOR (Jia et al., 2018), a negative regulator of autophagy (Ganley et al., 2009; Hosokawa et al., 2009; Jung et al., 2009; Saxton and Sabatini, 2017), thus helping to activate autophagic responses (Fujita et al., 2013; Jia et al., 2018; Maejima et al., 2013). AMPK is a positive regulator of autophagy (Egan et al., 2011; Kim et al., 2011), and Gal9 and the machinery delineated above could contribute to autophagic and LC3 responses during lysosomal damage. We observed by Optiprep membrane fractionations that, upon LLOMe treatment, LAMP2 moved to lighter fractions along with LC3B-II (Fig. 7C), likely reflecting membranous intermediates during autophagic clearance. These fractions were positive for Gal9 and AMPK $\alpha$ 1 (Fig. 7C), consistent with our LysoIP data (Figs. S1F and 6E).

Gal9KO<sup>Huh7</sup> cells displayed reduced levels of LC3B-II relative to WT Huh7 cells treated with LLOMe (Fig. 7D), and fewer puncta for autophagy markers ATG13, ATG16L1 and LC3B (Figs. S5J–M). This was complemented by Gal9 WT, but not by Gal9<sup>R65A/239A</sup> that cannot recognize glycans (Figs. 7E and S6A–B). A knockdown of USP9X in Gal9KO<sup>Huh7</sup> partially restored LC3B-II levels (Fig. 7F), and LC3 puncta response (Fig. 7G) to LLOMe. USP9X knockdown did not affect LC3 response in WT Huh7 cells, indicating that the effects of USP9X are manifested only in the absence of Gal9 (Fig. 7G). Similar effects of USP9X knockdowns were obtained with ATG13 and ATG16 (Figs. S6C and S6D).

Treatment of Huh7 and HeLa cells with the TAK1 inhibitor 5ZO reduced the LC3 response (Fig. 5D). Thus, Gal9 effectors and the lysosomal-damage response pathway controlled by Gal9 control autophagy during lysosomal damage (Fig. S6F).

Previous studies of endomembrane damage and galectin-controlled autophagic responses have established effects on microbial survival, with an emphasis on the roles of autophagic receptors (Thurston et al., 2012) receptor-regulators (Chauhan et al., 2016), E3 ligases (Chauhan et al., 2016; Cheng et al., 2017; Maejima et al., 2013), and mTOR (Jia et al., 2018). Earlier work has shown that immunological, pharmacological or physiological

(starvation) induction of autophagy can control *Mycobacterium tuberculosis* (*Mtb*), an intracellular pathogen causing endomembrane damage (Manzanillo et al., 2012), in macrophages (Gutierrez et al., 2004). Since here we established AMPK as a downstream effector of Gal9, and AMPK plays a role in activating autophagy (Egan et al., 2011; Kim et al., 2011), we determined its effects on autophagic control of intracellular microbes. A positive role of Gal9 in defense against *Mtb*, has already been established (Jayaraman et al., 2010; Zhu et al., 2005). We thus tested the effects of the Gal9 effector AMPK on intracellular survival of *Mtb* in macrophages using a previously established system for assaying autophagic control of intracellular *Mtb* (Chauhan et al., 2016; Chauhan et al., 2015) and found that primary bone marrow-derived macrophages (BMMs) from mice with Cre recombinase-induced AMPK loss via a CX3CR1-driven Cre-Lox system and AMPK $\alpha$ 1<sup>fl/fl</sup>/AMPK $\alpha$ 2<sup>fl/fl</sup>, displayed a reduced ability to control intracellular *Mtb* upon induction of autophagy, as compared to CX3CR1 Cre<sup>-</sup> AMPK-sufficient BMMs. This shows that AMPK is important for the autophagic control of *Mtb* in infected macrophages (Fig. S6E).

## DISCUSSION

This work defines the molecular mechanism of how cells recognize lysosomal injury and transduce this signal to AMPK. It deorphans TAK1's role in AMPK activation (Neumann, 2018) giving it a unifying biological context - the response to lysosomal damage. Along with other recent studies (Jia et al., 2018), this work affirms a major regulatory role of intracellular galectins converging on AMPK and mTOR, the master regulators of cellular metabolism and QC processes. Lysosomal damage, itself a subject for QC, has consequences on metabolism as reflected in the metabolomic changes observed here.

The mechanism of AMPK activation in response to lysosomal membrane damage depends on the process of galectin-directed ubiquitination. The cascade of events activating AMPK is triggered by exposure of exofacial glycans normally not in contact with the cytosol since the delimiting membrane is not breached. Once the membrane is damaged, these exposed "exoglycoepitopes" are accessed by cytosolic galectins to set off downstream events, with those initiated by Gal9 culminating in AMPK activation. This process depends on K63 ubiquitination of TAK1 (Herrero-Martin et al., 2009; Singhirunusorn et al., 2005; Xie et al., 2006). A previously characterized agonist of AMPK activation by TAK1 is TRAIL (Herrero-Martin et al., 2009). TRAIL is known to induce lysosomal permeabilization (Werneburg et al., 2007) reinforced by our observations. TAK1 responds to lysosomal rupture in the context of inflammasome activation (Okada et al., 2014). Thus, the unifying physiological context for AMPK activation by TAK1 is the lysosomal integrity status.

The canonical pathway for AMPK activation occurs via binding of AMP to its regulatory subunit  $\gamma$  during metabolic stress (Hardie, 2014). However, AMPK can detect glucose depletion before energy status changes using a non-canonical pathway localized to lysosomes that does not rely on AMP (Li et al., 2019; Lin and Hardie, 2018; Zhang et al., 2017; Zhang et al., 2014; Zhang et al., 2013). There are similarities and differences between the glucose-deprivation (Lin and Hardie, 2018) and the lysosome-damage signaling pathway described in our study as distinct non-canonical pathways occurring on lysosomes. The glucose starvation FBP-sensing pathway, which involves vATPase inhibition, depends on

LKB1 (Zhang et al., 2014), whereas the dominant kinase during lysosomal damage response of AMPK is TAK1. The lysosomally localized FBP-sensing pathway borrows parts of the mTOR regulatory machinery stationed on the lysosomes (Saxton and Sabatini, 2017) and is composed of the v-ATPase-Ragulator/LAMTOR1-AXIN-LKB1-AMPK complex (Lin and Hardie, 2018; Zhang et al., 2014). In contrast, the TAK1-AMPK activation pathway responding to lysosomal damage is anchored to the lysosomes by Gal9 after its recognition of membrane tears. Nevertheless, there may be lateral overlaps between the FBP-sensing and the lysosomal damage-sensing pathways. This is evidenced by detection in our LC-MS/MS experiments with LLOMe (Fig. 1G) of increased Gal9-LAMTOR1 and Gal9-vATPase subunit ATP6V1A associations, as well as additional interactions with other components, e.g. NPC1 (Castellano et al., 2017), of the lysosomal mTOR regulatory apparatus (Saxton and Sabatini, 2017).

AMPK activation is sensitive to duration and extent of lysosomal damage and diminishes past 30 min of massive damage leading to autophagy and lysophagy. We have considered the possibility that a mild lysosomal damage may be a physiologically relevant trigger for sustained activation AMPK and detected hallmarks of limited lysosomal damage during metformin treatment. Metformin, a widely used antidiabetic drug (He and Wondisford, 2015), is a known AMPK inducer believed to act by inhibiting complex I of the mitochondrial electron transport chain thus raising AMP levels (Foretz et al., 2014). Nevertheless, metformin's precise mode of action remains unclear, since activation of AMPK is not always supported by detection of AMP in metformin-treated cells (He and Wondisford, 2015). Furthermore, a plethora of effects is often invoked to explain metformin's mode of action and benefits (Hur and Lee, 2015; Rajani et al., 2017). Recent studies (Kim et al., 2016; Zhang et al., 2016) have implicated endolysosomal compartments in metformin action and it has been shown that metformin can induce AMPK through a lysosomal v-ATPase proposed to act as a sensor or an effector of metformin in AMPK activation (Zhang et al., 2016). In this model, metformin is suggested to engage the lysosomal FBP-sensing complex discussed above. Our metformin findings corroborate with the notion that lysosomal perturbations contribute to metformin's effects. However, as discussed above, the FBP-sensing and the Gal9-sensing pathways are distinct, as one operates in glucose metabolite sensing whereas the other detects lysosomal membrane damage. Indeed, we observed that metformin elicited ALIX puncta formation, with ALIX being a component of the ESCRT machinery engaged in membrane repair caused by very mild lysosomal damage (Radulovic et al., 2018; Skowyra et al., 2018). Thus, these responses may represent a physiologically relevant aspect for sustained AMPK activation by metformin.

The complexity of the landscape of known E3 ligases as well as their paucity (with the exception of TRIM25) in our proteomic analyses (Table S1, Tab 5) prevented us from investigating TAK1 ubiquitination from the perspective of E3 ligases. Instead, we noticed dynamic changes in DUBs and VCP/p97 and identified USP9X as a key Gal9-governed DUB regulating the TAK1 ubiquitination state. USP9X acts as a linchpin in the switch caused by Gal9 and lysosomal damage. Other DUBs have been implicated in acting on TAK1, including CYLD (Ji et al., 2018; Reiley et al., 2007), USP4 (Fan et al., 2011), USP14 (Min et al., 2017), USP18 (Yang et al., 2015) and USP19 (Lei et al., 2019). Of these, our

proteomic analyses with APEX2-Gal9 identified only USP19 but with low peptide counts below the threshold (Table S1, Tab 6).

Our study uncovers a specific control of ubiquitination responses by galectins. This underlies the TAK1-dependent activation of AMPK during lysosomal damage, a condition that we propose is a major physiological context for AMPK activation by TAK1. The Gal9-AMPK axis is important in medically relevant contexts, e.g. in *Mtb* control, as shown here for AMPK and elsewhere for Gal9 (Jayaraman et al., 2010; Zhu et al., 2005). A therapeutic utility of these relationships with implications for metabolic disorders, cancer, and other diseases is underscored by metformin's action suggestive of a need to develop drugs targeting lysosomal integrity and signaling. The findings reported here have broader implications for QC of cellular organelles, metabolic switching, cell physiology, and effector functions including autophagy and defense against intracellular pathogens.

## STAR METHODS

### LEAD CONTACT AND MATERIALS AVAILABILITY

Further information and requests for resources and reagents should be directed to and will be fulfilled by the Lead Contact, Vojo Deretic (vderetic@salud.unm.edu). All unique/stable reagents generated in this study are available from the Lead Contact with a completed Materials Transfer Agreement negotiated as governed by the University of New Mexico and state requirements and, where applicable, covering costs associated with preparation and shipping.

### EXPERIMENTAL MODEL AND SUBJECT DETAILS

**Human subjects**—Healthy adult volunteers (age 18–40, both sexes) were enrolled in a protocol approved by the Human Research Review Committee (administered by the Human Research Protections Office, University of New Mexico Health Sciences Center). Consented volunteers (informed consent was obtained from all subjects) donated up to 50 mL peripheral venous blood for isolation and culture of peripheral blood monocyte-derived macrophages

**Cell and cell line models**—Murine bone marrow derived macrophages (BMMs; primary cells) were used for *M. tuberculosis* infection analyses. Cell types, lines and culture conditions are described under Method Details.

**Mice**—The following information is included, as requested: “CX3CR1-driven Cre-Lox system AMPK $\alpha$ 1<sup>1/1</sup>/AMPK $\alpha$ 2<sup>1/1</sup> mice in C57/BL6, background (6–8 weeks old, both sexes) were the source of BMMs. These mice have been constructed and maintained at USC under approved breeding protocols and all experiments with BMMs were approved by the Institutional Animal Care and Use Committees

**Murine tuberculosis infection model**—*Mycobacterium tuberculosis* Erdman (Manzanillo et al., 2012) were cultured in Middlebrook 7H9 broth supplemented with 0.05 % Tween 80, 0.2 % glycerol, and 10 % oleic acid, albumin, dextrose, and catalase

(OADCBD Biosciences) at 37 °C and homogenized to generate single-cell suspension for macrophage infection studies.

## METHOD DETAILS

**Antibodies and reagents**—Antibodies from Cell Signaling Technology were used at 1:1000 for WB including p-AMPK $\alpha$  (#2535), AMPK $\alpha$  (#2532), p-ACC (#11818), ACC (#3662), p-ULK1 Ser555 (#5869), ULK1 (#6439), p-TAK1 (#4508), TAK1 (#5206), HA (#3724S), ATG13 (#13468) (1:200 for IF), LAMP1 (#9091) (1:500 for IF), AXIN (#2087). Antibodies from Abcam were Galectin 9 (ab69630; 1:500 WB; 1:100 IF), USP9x (ab19879; 1:1000 WB), GFP (ab290; 1:1000 WB), GFP (ab38689; 2  $\mu$ g/mL for immunoprecipitation (IP)), mCherry (ab183628; 1:1000 WB; 1:200 IF; 2  $\mu$ g/mL IP). VDAC1 (ab15895), GM130 (ab1299), PDI (ab2792), LKB1 (ab61122), CaMKK2 (ab96531), Cathepsin D (ab6313) were used at 1:1000 for WB. Antibodies from MBL International were LC3 (PM036) (1:500 for IF) and ATG16L1 (PM040) (1:400 for IF). Antibodies from BioLegend were Galectin 3 (#125402) (1:1000 for WB; 1:500 for IF). Other antibodies used in this study were from the following sources: Ubiquitin (FK-2) (Millipore 04–263; 1:1000 WB), Catalase (Calbiochem 219010; 1:1000 WB), Galectin 9 (R&D AF2045; 1:200 WB), FLAG M2 (Sigma Aldrich F1804; 1:1000 WB); Galectin 8 (sc-28254) (1:200 for WB; 1:100 IF), beta-Actin (C4) (1:1000 for WB), c-Myc (sc-40), HRP-labeled anti-rabbit (sc-2004; 1:2000 for WB) and anti-mouse (sc-2005, 1:2000 for WB) were from Santa Cruz Biotechnology; LAMP2 (H4B4) (1:500 for IF) from DSHB of University of Iowa; Clean-Blot IP Detection Kit (HRP) (21232) (1:1000 for WB), Alexa Fluor 488, 568 (1:500 for IF) were from ThermoFisher. ALIX (#634502, 1:1000 WB; 1:500 IF) were from BioLegend. Dynabeads Protein G (10003D), anti-HA Magnetic Beads (88836), streptavidin Magnetic Beads (88816), DMEM (no glucose, 11966025), RIPA and NP40 lysis buffer were from ThermoFisher. DMEM, RPMI and EBSS media were from Life Technologies. TAK1 inhibitor (5Z-oxozeanol) (O9890) Sigma.

**Cells and cell lines**—HEK293T cells stably expressing APEX2-GAL9 (APEX2-Gal9–293T<sup>stable</sup>) were obtained by lentiviral transduction followed by selection with antibiotics. Briefly, for virus generation, 1  $\mu$ g of pMD2.G and 2.7  $\mu$ g of pPAX2 retroviral packaging plasmid were transfected into HEK293T cells together with 3.3  $\mu$ g of pHAGE-Myc-APEX2-GAL9. Targeted HEK293T cells were transduced with virus containing medium, which was exchanged to growth medium after 24 h infection. Transduced cells were selected and cultured in Dulbecco's modified Eagle's medium (DMEM), supplemented by 10 % fetal bovine serum and 2  $\mu$ g/mL puromycin (Sigma). Target-gene expression was confirmed via SDS-PAGE and immunoblot. HEK293T, HeLa and Huh7 cells were obtained from ATCC. Bone marrow derived macrophages (BMMs) were isolated from femurs of AMPK $\alpha$ 1<sup>fl/fl</sup>/AMPK $\alpha$ 2<sup>fl/fl</sup> CX3CR1-Cre mice and their Cre-negative littermates cultured in DMEM supplemented with mouse macrophage colony stimulating factor (mM-CSF, #5228, CST). HeLa Flp-In-Gal9<sup>Tet-ON</sup> were generated using vectors and recipient cells from Terje Johansen (University of Norway). Cell lines for LysoIP were generated using constructs obtained from David M. Sabatini (Whitehead Institute). TAB2 KO MEFs were from Shizuo Akira (Osaka University). Gal9KO<sup>Huh7</sup> cells were generated using CRISPR in this study. The details for cell line generation is below.

**Cultured human peripheral blood monocyte cells**—A trained phlebotomist in our HRRC-approved study drew 40–50 mL blood from healthy, consenting adult volunteers enrolled in the study. The different donors were kept separate and the blood in 10 mL vacutainers was pooled into 2–50 mL conicals. The volume was brought to 50 mL with sterile 1X PBS and mixed by inversion. 25 mL of the blood mix were carefully layered onto 20 mL of Ficoll (Sigma, #1077) in separate conical tubes and centrifuged at 2000 rpm for 30 min at 22 °C. The buffer layer containing human peripheral blood monocytes (PBMCs) was removed, pooled, washed with 1X PBS twice and resuspended in ~20 mL RPMI media with 10 % human AB serum and Primocin.

**Plasmids, siRNAs, and transfection**—pRK5-HA-Ubiquitin-WT (Addgene#17608; mammalian expression of HA tagged ubiquitin), pRK5-HA-Ubiquitin-K48 (Addgene#17605; mammalian expression of HA tagged ubiquitin all lysines mutated to arginines except the K48 residue) and pRK5-HA-Ubiquitin-K63 (Addgene#17606; mammalian expression of HA tagged ubiquitin with all lysines mutated to arginines except the K63); see Key resources table. For proximity proteomics, human GAL9 was cloned into pHAGE-Myc-APEX2 using Gateway cloning (ThermoFisher). Gal9 mutants were generated utilizing the QuikChange site-directed mutagenesis kit (Agilent) and confirmed by sequencing (Genewiz). siRNAs were from GE Dharmacon. Plasmid transfections were performed using the ProFection Mammalian Transfection System (Promega), Amaxa nucleofection (Lonza) or Lipofectamine 2000 (ThermoFisher). siRNAs were delivered into cells using either Lipofectamine RNAiMAX (ThermoFisher) or Amaxa nucleofection (Lonza).

**Generation of Galectin 9 CRISPR mutant cells**—For generating Gal9 CRISPR mutant cells, the lentiviral vector lentiCRISPRv2 carrying both Cas9 enzyme and a gRNA targeting Gal9 (gRNA target sequence: ACACACACACCTGGTTCCAC) was transfected into HEK293T cells together with the packaging plasmids psPAX2 and pCMV-VSV-G at the ratio of 5:3:2. Two days after transfection, the supernatant containing lentiviruses was collected and used to infect Huh7 cells. 36 h after infection, the cells were selected with puromycin (1 µg/mL) for one week in order to select Gal9 knockout cells. Gal9 knockout was confirmed by western blot. Selection of single clones was performed by dilution in 96-well, which were confirmed by western blots (Figs. S1C and S1D).

**Generating HeLa Flp-In-Gal9<sup>Tet-ON</sup> cell line**—HeLa Flp-In host cells were transfected with Gal9 reconstructed plasmid and the pOG44 expression plasmid at ratio of 9:1. 24 h after transfection, the cells were washed, and cultured in fresh medium. 48 h after transfection, the cells were split into fresh medium at around 25 % confluency. The cells are incubated at 37 °C for 2–3 h until they have attached to the culture dish. Then medium was removed and fresh medium containing 100 µg/mL hygromycin was added. The cells were fed with selective medium every 3–4 days until single cell clone can be identified. Hygromycin-resistant clones were picked and expanded each to test. The tested clones were incubated in the medium containing 1 µg/mL tetracycline overnight and were tested by western blot for the expression of Gal9.

**LysoIP immunoblot assay**—Stable LysoIP cells were produced by utilizing lentiviruses constructs from David M. Sabatini Lab (Whitehead Institute) following published protocols (Abu-Remaileh et al., 2017). HEK293T cells were transfected with pLJC5-TMEM192-3XHA or pLJC5-TMEM192-2XFLAG constructs in combination with pCMV-VSV-G and psPAX2 packaging plasmids, 60 h after transfection, the supernatant containing lentiviruses was collected and centrifuged to remove cells and then frozen at  $-80^{\circ}\text{C}$ . To establish LysoIP stably expressing cell lines, HEK293T, Huh7 or Huh7 Gal9<sup>KO</sup> cells were plated in 10 cm<sup>2</sup> dish in DMEM with 10 % FBS and infected with 500  $\mu\text{L}$  of virus-containing media overnight followed by addition of 1  $\mu\text{g}/\text{mL}$  puromycin for selection. Cells were plated in 15 cm<sup>2</sup> culture plates and were used at 90 % confluency for each LysoIP. Cells with or without 1 mM LLOMe treatment were quickly rinsed twice with PBS and then scraped in 1 mL of KPBS (136 mM KCl, 10 mM KH<sub>2</sub>PO<sub>4</sub>, pH7.25 was adjusted with KOH) and centrifuged at 3000 rpm for 2 min at 4  $^{\circ}\text{C}$ . Pelleted cells were resuspended in 950  $\mu\text{L}$  KPBS and reserved 25  $\mu\text{L}$  for further processing of the whole-cell lysate. The remaining cells were gently homogenized for 20 strokes using a 2 mL homogenizer. The homogenate was then centrifuged at 3000 rpm for 2 min at 4  $^{\circ}\text{C}$  and the supernatant was incubated with 100  $\mu\text{L}$  of KPBS prewashed anti-HA magnetic beads (ThermoFisher) on a gentle rotator shaker for 3 min. Immunoprecipitants were then gently washed three times with KPBS and eluted with 2X Laemmli sample buffer (Bio-Rad) and subjected to immunoblot analysis.

***M. tuberculosis* survival in murine bone marrow-derived macrophages**—

*Mycobacterium tuberculosis* Erdman (Erdman) culture was prepared by thawing frozen stock aliquot and grown in 7H9 Middlebrook liquid medium supplemented with oleic acid, albumin, dextrose and catalase (OADC, Becton Dickinson, Inc., Sparks, MD, USA), 0.5 % glycerol and 0.05 % Tween 80. Cultures were grown at 37  $^{\circ}\text{C}$ . BMMs were infected with Erdman at MOI 10 and incubated for 18 h (in full medium for 18 h, or for starvation, in full medium for 16 h followed by 2 h in EBSS) lysed and plated on 7H11 agar plates. CFU was enumerated 3 ~ 4 weeks later.

**High content microscopy**—The cells were plated in 96 well plates on day 1 and were treated on day 2, followed by fixation in 4 % paraformaldehyde for 5 min. After fixation, cells were washed twice with 1X PBS and were then permeabilized with 0.1 % saponin in 3 % Bovine serum albumin (BSA) for 30 min. The cells were then incubated with primary antibodies overnight at 4  $^{\circ}\text{C}$ . On day 3, the cells were washed twice with 1X PBS and incubated with secondary antibodies for 1h followed by 5 min incubation with Hoechst 33342. High content microscopy with automated image acquisition and quantification was carried out using a Cellomics HCS scanner and iDEV software (ThermoFisher). Automated epifluorescence image collection was performed for a minimum of 500 cells per well. Epifluorescence images were machine analyzed using preset scanning parameters and object mask definitions. Hoechst 33342 staining was used for autofocus and to automatically define cellular outlines based on background staining of the cytoplasm. Primary objects were cells, and regions of interest (ROI) or targets were algorithm-defined by shape/segmentation, maximum/minimum average intensity, total area and total intensity, etc., to automatically identify puncta or other profiles within valid primary objects. All data collection, processing

(object, ROI, and target mask assignments) and analyses were computer driven independently of human operators.

**Immunofluorescence confocal microscopy**—For immunofluorescence confocal microscopy, cells were plated onto coverslips in 12 well or 24 well plates. Cells were transfected with plasmids as indicated in figures. Cells were incubated in full media or EBSS for 2 h and fixed in 4 % paraformaldehyde for 10 min followed by permeabilization with 0.1 % saponin in 3 % BSA. Cells were then blocked in 3 % BSA and then stained with primary antibodies followed by washings with PBS and then incubation with appropriate secondary antibodies for 1 h at room temperature. Coverslips were mounted using ProLong Gold Antifade Mountant (Invitrogen) and analyzed by confocal microscopy using the Zeiss LSM510 Laser Scanning Microscope.

**Membrane fractionation**—Membrane fractionation was performed as described previously (Ge et al., 2013). HEK293T cells (10 dishes per sample) were plated in 15-cm<sup>2</sup> dishes and treated with 1mM LLOMe for 30 min. For sequential centrifugation cells were harvested, and the pellet was resuspended in 2.7X cell pellet volume of B1 buffer (20 mM Hepes-KOH, pH 7.2, 400 mM sucrose, and 1 mM EDTA) containing protease and phosphatase inhibitors (Roche) and 0.3 mM DTT and then was homogenized by passing through a 22-G needle until 85–90 % lysis was achieved (analyzed by trypan blue staining). Homogenates were subjected to sequential differential centrifugation at 3,000 g for 10 min, 25,000 g for 20 min, and 100,000 g for 30 min to collect the pelleted membranes (3K, 25K, and 100K, respectively) using a TLA100.3 rotor (Beckman Coulter) and a polypropylene tube. The pellets were suspended in B88 buffer (20 mM Hepes, pH 7.2, 150 mM potassium acetate, 5 mM magnesium acetate, and 250 mM sorbitol). 5X SDS loading buffer was added, and samples were boiled for 5 min and analyzed by immunoblotting. Further fractionation using membrane floatation in a sucrose step gradient followed by centrifugation in OptiPrep step gradients was performed as described previously (Ge et al., 2013). For this, 25K membrane pellets were suspended in 1 mL of 19 % OptiPrep for a step gradient containing 0.5 mL of 22.5 %, 1 mL of 19 % (sample), 0.9 mL of 16 %, 0.9 mL of 12 %, 1 mL of 8 %, 0.5 mL of 5 %, and 0.2 mL of 0 % OptiPrep each. The OptiPrep gradient was centrifuged at 150,000 g for 3 h, and subsequently, eight fractions of 0.5 ml each were collected from the top. Fractions were diluted with B88 buffer, and membranes were collected by centrifugation at 100,000 g for 1 h. Samples were subjected to SDS-PAGE, and Western blotting for LAMP2, AMPK $\alpha$ , myc-Gal9 and LC3B was done as described in the following section.

**Immunoblotting and Co-immunoprecipitation assay**—Western blotting and co-immunoprecipitation (co-IP) were performed as described previously (Chauhan et al., 2016). For TAK1 inhibition, the cells were treated with TAK1 inhibitor (5Z-oxozeanol) 1 h prior to LLOMe treatment. For co-IP, cells were transfected with plasmids as indicated in figures and lysed in NP-40 buffer containing protease inhibitor cocktail and PMSF. Lysates were incubated with antibodies for 4 h at 4 °C followed by incubation with protein G Dynabeads for 2 h at 4 °C. Beads were washed three times with 1X PBS and boiled with SDS

containing sample buffer, samples were processed for immunoblotting to analyze the interactions between immunoprecipitated proteins.

**BioWeb (APEX2-labeling proximity biotinylation and Western blotting)—**

HEK293T cells transfected with indicated plasmid or APEX2-Gal9-293T<sup>stable</sup> cells were incubated with 1 mM LLOMe in full medium for 30 min (confluence of cells remained at 70–80 %) and 500  $\mu$ M biotin-phenol (AdipoGen) in full medium for 30 min with LLOMe incubation. A 1 min pulse with 1 mM H<sub>2</sub>O<sub>2</sub> at room temperature was stopped with quenching buffer (10 mM sodium ascorbate, 10 mM sodium azide and 5 mM Trolox in Dulbecco's Phosphate Buffered Saline (DPBS)). All samples were washed twice with quenching buffer, and twice with DPBS.

Cell pellets were lysed in 500  $\mu$ L ice-cold lysis buffer (6 M urea, 0.3 M NaCl, 1 mM EDTA, 1 mM EGTA, 10 mM sodium ascorbate, 10 mM sodium azide, 5 mM Trolox, 1 % glycerol and 25 mM Tris/HCl, PH 7.5) for 30 min by gentle pipetting. Lysates were clarified by centrifugation and protein concentrations determined as above. Streptavidin-coated magnetic beads (Pierce) were washed with lysis buffer. 3 mg of each sample was mixed with 100  $\mu$ L of streptavidin bead. The suspensions were gently rotated at 4 °C for overnight to bind biotinylated proteins. The flowthrough after enrichment was removed and the beads were washed in sequence with 1 mL IP buffer (150 mM NaCl, 10 mM Tris-HCl pH8.0, 1 mM EDTA, 1 mM EGTA, 1 % Triton X-100) twice; *1 mL 1M KCl; 1mL of 50 mM Na<sub>2</sub>CO<sub>3</sub>; 1 mL 2M Urea in 20 mM Tris HCl pH8; 1 mL IP buffer.* Biotinylated proteins were eluted, and *the sample were processed for Western Blot.*

**LysoTracker assay**—Prepare fresh LysoTracker Staining Solution (2  $\mu$ L LysoTracker in 1mL medium). Add 10  $\mu$ L LysoTracker Staining Solution to no treatment, LLOMe treated or Metformin treated THP-1 cells in 96 wells for total 100  $\mu$ L per well and incubate at 37 °C for 30 min protected from light. Rinse gently by 1X PBS and fix in 4 % Paraformaldehyde for 2 min. Wash once by 1X PBS and blot with Hoechst 33342 for 2 min before detecting by high content microscopy.

**Magic Red assay**—Reconstitute Magic Red by adding DMSO and dilute Magic Red 1:10 by adding H<sub>2</sub>O. Add 4  $\mu$ L Magic Red to no treatment, LLOMe treated or Metformin treated THP-1 cells in 96 wells for total 100  $\mu$ L per well and incubate at 37 °C for 15 min and protected from light. Rinse gently by 1X PBS and fix in 4 % Paraformaldehyde for 2 min. Wash once by 1X PBS and blot with Hoechst 33342 for 2 min before detecting by high content microscopy.

**AMP/ATP assay**—10<sup>5</sup> huh7 cells per sample, subjected to the 1mM LLOMe treatment for different time, was prepared for the extraction, following the boiling water method (Yang et al., 2002), the ratio of AMP and ATP were measured using ATP/ADP/AMP Assay Kit (Biomedical Research Service & Clinical Application). The luciferase bioluminescence was measured using a Synergy HTX Multi-Mode Reader. Data is normalized by the protein level of each sample.

## Proteomic mass spectrometry, data processing and analysis

**(i) SILAC Labelling and treatment for proteomic analyse:** HEK293T cells stably expressing APEX2-GAL9 were grown in lysine- and arginine-free DMEM supplemented with fetal bovine serum (FBS), L-Glutamine, Sodium pyruvate, heavy arginine (R10) (38 µg/mL) and lysine (K8) (66 µg/mL) or light arginine (R0) (38 µg/mL) and lysin (K0) (66 µg/mL), respectively. Further experiments were conducted as soon as the cells reached a protein labelling with heavy amino acids of at least 95 %. Heavy-labeled cells were either treated with 1 mM Leu-Leu methyl ester hydrobromide (LLOMe, Sigma) for 1 h or with 100 µM Gly-Phe β-naphthylamide (GPN, Sigma) for 1h at 37 °C while light-labelled cells were treated with control (DMSO).

**(ii) Proximity Labeling for proteomic mass spectrometry:** Proximity labeling was performed in SILAC labelled HEK293T cells stably expressing APEX2-GAL9 as described before (Le Guerroue et al., 2017). Briefly, cells were incubated with 500 µM Biotin-Phenol during the last 30 min of LLOMe or GPN treatment and subsequently pulsed by addition of H<sub>2</sub>O<sub>2</sub> for 1 min at room temperature. To stop the biotinylation reaction, they were washed 3 times with quencher solution (10 mM sodium azide, 10 mM sodium ascorbate, 5 mM Trolox in DPBS) and 3 times with PBS. All further steps were performed at 4°C unless indicated otherwise. After cell harvest with 0.25 % Trypsin/EDTA (ThermoFisher), cells were counted and heavy- and light-labelled cells were mixed at a 1:1 ratio based on total cell numbers. After centrifugation, the resulting cell pellets were lysed in RIPA (50 mM Tris, 150 mM NaCl, 0.1 % SDS, 1 % Triton X-100, 0.5 % sodium deoxycholate) supplemented with 10 mM sodium ascorbate, 1 mM sodium azide, 1 mM Trolox and protease inhibitors (Roche Complete). Samples were sonicated 2 times for 1 s, spun down at 10,000 g for 10 min before application to streptavidin agarose resin (ThermoFisher) and incubation with overhead shaking overnight.

**(iii) Proteomic mass spectrometry after proximity biotinylation:** IP-MS was performed as described before (Lobingier et al., 2017). Briefly, samples were washed 3 times in RIPA buffer and 3 times in 3 M Urea buffer (in 50 mM ABC) followed by incubation with TCEP (5 mM final) for 30 min at 55 °C with orbital shaking. After alkylation with IAA (10 mM final) for 20 min at room temperature in the dark the reaction was quenched with DTT (20 mM final). Samples were washed 2 times with 2M Urea (in 50 mM ABC) before trypsin digestion overnight at 37 °C (20 µg/mL final). The resin was spun down and supernatants containing digested peptides were collected. After washing the resin 2 times with 2 M Urea and pooling all supernatants the samples were acidified with TFA (1 % final). Digested peptides were desalted on custom-made C18 stage tips. Using an Easy-nLC1200 liquid chromatography, peptides were loaded onto 75 µm × 15 cm fused silica capillaries (New Objective) packed with C18AQ resin (Reprosil- Pur 120, 1.9 µm, Dr. Maisch HPLC). Peptide mixtures were separated using a gradient of 5 %–33 % acetonitrile in 0.1 % acetic acid over 35 min and detected on an Orbitrap Elite mass spectrometer (ThermoFisher). Dynamic exclusion was enabled for 30 s and singly charged species or species for which a charge could not be assigned were rejected. MS data was processed and analyzed using MaxQuant (version 1.6.0.1) (Cox and Mann, 2008) and Perseus (version 1.5.8.4) (Tyanova et al., 2016). All proximity experiments were performed in triplicates. Unique and razor

peptides were used for semiquantitative analyses. Matches to common contaminants, reverse identifications and identifications based only on site-specific modifications were removed prior to further analysis. Log<sub>2</sub> Heavy/Light ratios were calculated. A threshold based on a log<sub>2</sub> fold change of greater than 1-fold or less than -1-fold was chosen so as to focus the data analysis on a smaller set of proteins with the largest alterations in abundance. MATLAB software was used to generate volcano plots. Student t-tests were used to determine statistical significance between treatments. A p-value < 0.05 was considered statistically significant. Raw MS data are available from ProteomeXchange. Project Name: SILAC APEX2-GAL9 upon LLOMe or GPN treatment; Project accession: PXD015779.

**Metabolomic analyses by CE-Qq/TOFMS CE-MS/MS**—Cultured cells (10<sup>6</sup> cells/sample) were used for the extraction of intracellular metabolites. The culture medium was aspirated from the dish and cells were washed twice by 5 % mannitol solution (10 mL first and then 2 mL). The cells were then treated with 800 μL of methanol and left at rest for 30 s in order to inactivate enzymes. Next, the cell extract was treated with 550 μL of Milli-Q water containing internal standards (H3304–1002, Human Metabolome Technologies, Inc., Tsuruoka, Japan) and left at rest for another 30 s. The extract was obtained and centrifuged at 2,300 g and 4 °C for 5 min and then 800 μL of upper aqueous layer was centrifugally filtered through a Millipore 5-kDa cutoff filter at 9,100 g and 4 °C for 120 min to remove proteins. The filtrate was centrifugally concentrated and re-suspended in 50 μL of Milli-Q water for CE-MS analysis. Cationic compounds were measured in the positive mode of CE-TOFMS and anionic compounds were measured in the positive and negative modes of CE-MS/MS according to the methods developed by Soga, et al (Soga and Heiger, 2000; Soga et al., 2003; Soga et al., 2002). Peaks detected by CE-TOFMS and CE-MS/MS were extracted using automatic integration software (MasterHands, Keio University, Tsuruoka, Japan (Sugimoto et al., 2010) and MassHunter Quantitative Analysis B.04.00, Agilent Technologies, Santa Clara, CA, USA, respectively) in order to obtain peak information including m/z, migration time (MT), and peak area. The peaks were annotated with putative metabolites from the HMT metabolite database based on their MTs in CE and m/z values determined by TOFMS. The tolerance range for the peak annotation was configured at ±0.5 min for MT and ±10 ppm for m/z. In addition, concentrations of metabolites were calculated by normalizing the peak area of each metabolite with respect to the area of the internal standard and by using standard curves, which were obtained by three-point calibrations. Hierarchical cluster analysis (HCA) and principal component analysis (PCA) were performed by PeakStat and SampleStat software, respectively. Detected metabolites were plotted on metabolic pathway maps using VANTED (Visualization and Analysis of Networks containing Experimental Data) software (Junker et al., 2006).

**LysoIP proteomic analysis and DIA quantification and statistical analysis**—Freshly generated stable LysoIP HEK293T cells were generated as described in the LysoIP section by transduction with lentiviruses (prepared from HEK293T cells co-transfected with pLJC5-TMEM192-3XHA in combination with pCMV-VSV-G and psPAX2 packaging plasmids). Unlike for standard LysoIP where established stable cell lines were employed, for LysoIP proteomic studies only freshly generated stable cells were used. The cells were subjected to lysosomal damage with 1 mM LLOMe for 30 min, lysosomes purified

following the LysoIP protocol (Abu-Remaileh et al., 2017). Beads with bound lysosomes were washed four times with 200  $\mu$ L of 50mM Triethyl ammonium bicarbonate (TEAB) with a 20 min shake time at 4  $^{\circ}$ C in between each wash. Roughly 2.5  $\mu$ g of trypsin was added to the bead and TEAB mixture and the samples were digested over night at 800 rpm shake speed. After overnight digestion the supernatant was removed, and the beads were washed once with enough 50 mM ammonium bicarbonate to cover. After 20 min at a gentle shake the wash is removed and combined with the initial supernatant. The peptide extracts are reduced in volume by vacuum centrifugation and a small portion of the extract is used for fluorometric peptide quantification (Thermo scientific Pierce). One microgram of sample based on the fluorometric peptide assay was loaded for each LC/MS analysis.

Peptides were separated on an Easy-spray 100  $\mu$ m  $\times$  25 cm C18 column using a Dionex Ultimate 3000 nUPLC. Solvent A=0.1 % formic acid, Solvent B=100 % Acetonitrile 0.1 % formic acid. Gradient conditions = 2 %B to 50 %B over 60 min, followed by a 50 %–99 % B in 6 min and then held for 3 min than 99 %B to 2 %B in 2 min. Total Run time = 90 min. Thermo Scientific Fusion Lumos mass spectrometer running in Data independent Analysis mode. Two gas phases fractionated (GFP) injections were made per sample using sequential 4 Da isolation widows. GFP1 = m/z 362–758, GFP 2 = m/z 758–1158. Tandem mass spectra were acquired using a collision energy of 30, resolution of 30K, maximum inject time of 54 ms and a AGC target of 50K.

DIA data was analyzed using Scaffold DIA (1.3.1). Raw data files were converted to mzML format using ProteoWizard (3.0.11748). Analytic samples were aligned based on retention times and individually searched against *Pan human library* <http://www.swathatlas.org/> with a peptide mass tolerance of 10.0 ppm and a fragment mass tolerance of 10.0 ppm. Variable modifications considered were: Modification on M M and Modification on C C. The digestion enzyme was assumed to be Trypsin with a maximum of 1 missed cleavage site(s) allowed. Only peptides with charges in the range <2..3> and length in the range <6..30> were considered. Peptides identified in each sample were filtered by Percolator (3.01.nightly-13–655e4c7-dirty) to achieve a maximum FDR of 0.01. Individual search results were combined and peptide identifications were assigned posterior error probabilities and filtered to an FDR threshold of 0.01 by Percolator (3.01.nightly-13–655e4c7-dirty).

Peptide quantification was performed by Encyclopedia (0.8.1). For each peptide, the 5 highest quality fragment ions were selected for quantitation. Proteins that contained similar peptides and could not be differentiated based on MS/MS analysis were grouped to satisfy the principles of parsimony. Proteins with a minimum of 2 identified peptides were thresholded to achieve a protein FDR threshold of 1.0 %.

## QUANTIFICATION AND STATISTICAL ANALYSIS

Data are expressed as means  $\pm$  SEM (n = 3). Data were analyzed with a paired two-tailed Student's *t*-test or analysis of variance (ANOVA) was used. Statistical significance was defined as  $\dagger$ p > 0.05; \*p < 0.05, \*\*p < 0.01. Prism 8 or KaleidaGraph (v4.1.3.) software packages were used for statistical analysis. Power analysis was done only for HCM, based on previously published data using medium size effects. Replication, biological replicates (n) are indicated in legends. Error bars refer to biological replicates (technical sampling

errors not shown). Strategy for randomization and/or stratification, not applicable. Blinding was not used at any stage of the study: HCM analyses are machine and algorithm-driven image acquisition and data collection, processing and analyses and are investigator-independent processes. Inclusion and exclusion criteria, all data that passed technical criteria were included.

## DATA AND CODE AVAILABILITY

Original microscopy and Western blots of this study have been deposited at Mendeley data: <http://dx.doi.org/10.17632/4gb6s7mhh7.1>; Raw MS data are available from ProteomeXchange. Project Name: SILAC APEX2-GAL9 upon LLOMe or GPN treatment; Project accession: PXD015779.

## ADDITIONAL RESOURCES

None.

## Supplementary Material

Refer to Web version on PubMed Central for supplementary material.

## ACKNOWLEDGMENTS

This work was supported by NIH grants R37AI042999, R01AI042999 and a center grant P20GM121176 to V.D. M.R.B was partially supported by NCATS # U11TR001449. C.B. was supported by the Deutsche Forschungsgemeinschaft (DFG) within the framework of the Munich Cluster for Systems Neurology (EXC2145 SyNergy) and the Collaborative Research Center (CRC1177) as well as by the Boehringer Ingelheim Foundation.

## REFERENCES

- Abu-Remaileh M, Wyant GA, Kim C, Laqtom NN, Abbasi M, Chan SH, Freinkman E, and Sabatini DM (2017). Lysosomal metabolomics reveals V-ATPase- and mTOR-dependent regulation of amino acid efflux from lysosomes. *Science* 358, 807–813. [PubMed: 29074583]
- Aits S, Krickler J, Liu B, Ellegaard AM, Hamalisto S, Tvingsholm S, Corcelle-Termeau E, Hogh S, Farkas T, Holm Jonassen A, et al. (2015). Sensitive detection of lysosomal membrane permeabilization by lysosomal galectin puncta assay. *Autophagy* 11, 1408–1424. [PubMed: 26114578]
- Al-Hakim AK, Zagorska A, Chapman L, Deak M, Pegg M, and Alessi DR (2008). Control of AMPK-related kinases by USP9X and atypical Lys(29)/Lys(33)-linked polyubiquitin chains. *The Biochemical journal* 411, 249–260. [PubMed: 18254724]
- An H, and Harper JW (2018). Systematic analysis of ribophagy in human cells reveals bystander flux during selective autophagy. *Nature cell biology* 20, 135–143. [PubMed: 29230017]
- Arhzaouy K, Papadopoulos C, Schulze N, Pittman SK, Meyer H, and Wehl CC (2019). VCP maintains lysosomal homeostasis and TFEb activity in differentiated skeletal muscle. *Autophagy* 15, 1082–1099. [PubMed: 30654731]
- Berg TO, Stromhaug E, Lovdal T, Seglen O, and Berg T (1994). Use of glycyl-L-phenylalanine 2-naphthylamide, a lysosome-disrupting cathepsin C substrate, to distinguish between lysosomes and prelysosomal endocytic vacuoles. *The Biochemical journal* 300 (Pt 1), 229–236. [PubMed: 8198538]
- Bjorkoy G, Lamark T, Brech A, Outzen H, Perander M, Overvatn A, Stenmark H, and Johansen T (2005). p62/SQSTM1 forms protein aggregates degraded by autophagy and has a protective effect on huntingtin-induced cell death. *The Journal of cell biology* 171, 603–614. [PubMed: 16286508]

- Castellano BM, Thelen AM, Moldavski O, Feltes M, van der Welle RE, Mydock-McGrane L, Jiang X, van Eijkeren RJ, Davis OB, Louie SM, et al. (2017). Lysosomal cholesterol activates mTORC1 via an SLC38A9-Niemann-Pick C1 signaling complex. *Science* 355, 1306–1311. [PubMed: 28336668]
- Chauhan S, Kumar S, Jain A, Ponpuak M, Mudd MH, Kimura T, Choi SW, Peters R, Mandell M, Bruun JA, et al. (2016). TRIMs and Galectins Globally Cooperate and TRIM16 and Galectin-3 Co-direct Autophagy in Endomembrane Damage Homeostasis. *Developmental cell* 39, 13–27. [PubMed: 27693506]
- Chauhan S, Mandell MA, and Deretic V (2015). IRGM Governs the Core Autophagy Machinery to Conduct Antimicrobial Defense. *Molecular cell* 58, 507–521. [PubMed: 25891078]
- Cheng YL, Wu YW, Kuo CF, Lu SL, Liu FT, Anderson R, Lin CF, Liu YL, Wang WY, Chen YD, et al. (2017). Galectin-3 Inhibits Galectin-8/Parkin-Mediated Ubiquitination of Group A Streptococcus. *mBio* 8.
- Criollo A, Niso-Santano M, Malik SA, Michaud M, Morselli E, Marino G, Lachkar S, Arkhipenko AV, Harper F, Pierron G, et al. (2011). Inhibition of autophagy by TAB2 and TAB3. *The EMBO journal* 30, 4908–4920. [PubMed: 22081109]
- Deretic V, Saitoh T, and Akira S (2013). Autophagy in infection, inflammation and immunity. *Nat Rev Immunol* 13, 722–737. [PubMed: 24064518]
- Dikic I, and Elazar Z (2018). Mechanism and medical implications of mammalian autophagy. *Nature reviews Molecular cell biology* 19, 349–364. [PubMed: 29618831]
- Dupont N, Chauhan S, Arko-Mensah J, Castillo EF, Masedunskas A, Weigert R, Robenek H, Proikas-Cezanne T, and Deretic V (2014). Neutral lipid stores and lipase PNPLA5 contribute to autophagosome biogenesis. *Current biology : CB* 24, 609–620. [PubMed: 24613307]
- Dupont N, Lacas-Gervais S, Bertout J, Paz I, Freche B, Van Nhieu GT, van der Goot FG, Sansonetti PJ, and Lafont F (2009). Shigella phagocytic vacuolar membrane remnants participate in the cellular response to pathogen invasion and are regulated by autophagy. *Cell Host Microbe* 6, 137–149. [PubMed: 19683680]
- Egan DF, Shackelford DB, Mihaylova MM, Gelino S, Kohnz RA, Mair W, Vasquez DS, Joshi A, Gwinn DM, Taylor R, et al. (2011). Phosphorylation of ULK1 (hATG1) by AMP-activated protein kinase connects energy sensing to mitophagy. *Science* 331, 456–461. [PubMed: 21205641]
- Elgendy M, Ciro M, Abdel-Aziz AK, Belmonte G, Dal Zuffo R, Mercurio C, Miracco C, Lanfrancone L, Foiani M, and Minucci S (2014). Beclin 1 restrains tumorigenesis through Mcl-1 destabilization in an autophagy-independent reciprocal manner. *Nature communications* 5, 5637.
- Fan Y, Yu Y, Shi Y, Sun W, Xie M, Ge N, Mao R, Chang A, Xu G, Schneider MD, et al. (2010). Lysine 63-linked polyubiquitination of TAK1 at lysine 158 is required for tumor necrosis factor alpha- and interleukin-1beta-induced IKK/NF-kappaB and JNK/AP-1 activation. *The Journal of biological chemistry* 285, 5347–5360. [PubMed: 20038579]
- Fan YH, Yu Y, Mao RF, Tan XJ, Xu GF, Zhang H, Lu XB, Fu SB, and Yang J (2011). USP4 targets TAK1 to downregulate TNFalpha-induced NF-kappaB activation. *Cell death and differentiation* 18, 1547–1560. [PubMed: 21331078]
- Foretz M, Guigas B, Bertrand L, Pollak M, and Viollet B (2014). Metformin: from mechanisms of action to therapies. *Cell metabolism* 20, 953–966. [PubMed: 25456737]
- Fujita N, Morita E, Itoh T, Tanaka A, Nakaoka M, Osada Y, Umemoto T, Saitoh T, Nakatogawa H, Kobayashi S, et al. (2013). Recruitment of the autophagic machinery to endosomes during infection is mediated by ubiquitin. *The Journal of cell biology* 203, 115–128. [PubMed: 24100292]
- Gaber T, Strehl C, and Buttgerit F (2017). Metabolic regulation of inflammation. *Nat Rev Rheumatol* 13, 267–279. [PubMed: 28331208]
- Gack MU, Shin YC, Joo CH, Urano T, Liang C, Sun L, Takeuchi O, Akira S, Chen Z, Inoue S, et al. (2007). TRIM25 RING-finger E3 ubiquitin ligase is essential for RIG-I-mediated antiviral activity. *Nature* 446, 916–920. [PubMed: 17392790]
- Ganley IG, Lam du H, Wang J, Ding X, Chen S, and Jiang X (2009). ULK1.ATG13.FIP200 complex mediates mTOR signaling and is essential for autophagy. *The Journal of biological chemistry* 284, 12297–12305. [PubMed: 19258318]
- Garcia D, and Shaw RJ (2017). AMPK: Mechanisms of Cellular Energy Sensing and Restoration of Metabolic Balance. *Molecular cell* 66, 789–800. [PubMed: 28622524]

- Garin J, Diez R, Kieffer S, Dermine JF, Duclos S, Gagnon E, Sadoul R, Rondeau C, and Desjardins M (2001). The phagosome proteome: insight into phagosome functions. *The Journal of cell biology* 152, 165–180. [PubMed: 11149929]
- Gutierrez MG, Master SS, Singh SB, Taylor GA, Colombo MI, and Deretic V (2004). Autophagy is a defense mechanism inhibiting BCG and Mycobacterium tuberculosis survival in infected macrophages. *Cell* 119, 753–766. [PubMed: 15607973]
- Hansen M, Rubinsztein DC, and Walker DW (2018). Autophagy as a promoter of longevity: insights from model organisms. *Nature reviews Molecular cell biology* 19, 579–593. [PubMed: 30006559]
- Hardie DG (2011). AMP-activated protein kinase: an energy sensor that regulates all aspects of cell function. *Genes Dev* 25, 1895–1908. [PubMed: 21937710]
- Hardie DG (2014). AMPK--sensing energy while talking to other signaling pathways. *Cell metabolism* 20, 939–952. [PubMed: 25448702]
- Hawley SA, Pan DA, Mustard KJ, Ross L, Bain J, Edelman AM, Frenguelli BG, and Hardie DG (2005). Calmodulin-dependent protein kinase kinase-beta is an alternative upstream kinase for AMP-activated protein kinase. *Cell metabolism* 2, 9–19. [PubMed: 16054095]
- He L, and Wondisford FE (2015). Metformin action: concentrations matter. *Cell metabolism* 21, 159–162. [PubMed: 25651170]
- Heneka MT, Kummer MP, Stutz A, Delekate A, Schwartz S, Vieira-Saecker A, Griep A, Axt D, Remus A, Tzeng TC, et al. (2013). NLRP3 is activated in Alzheimer's disease and contributes to pathology in APP/PS1 mice. *Nature* 493, 674–678. [PubMed: 23254930]
- Herrero-Martin G, Hoyer-Hansen M, Garcia-Garcia C, Fumarola C, Farkas T, Lopez-Rivas A, and Jaattela M (2009). TAK1 activates AMPK-dependent cytoprotective autophagy in TRAIL-treated epithelial cells. *The EMBO journal* 28, 677–685. [PubMed: 19197243]
- Herzig S, and Shaw RJ (2018). AMPK: guardian of metabolism and mitochondrial homeostasis. *Nature reviews Molecular cell biology* 19, 121–135. [PubMed: 28974774]
- Hosokawa N, Hara T, Kaizuka T, Kishi C, Takamura A, Miura Y, Iemura S, Natsume T, Takehana K, Yamada N, et al. (2009). Nutrient-dependent mTORC1 association with the ULK1-Atg13-FIP200 complex required for autophagy. *Mol Biol Cell* 20, 1981–1991. [PubMed: 19211835]
- Hur KY, and Lee MS (2015). New mechanisms of metformin action: Focusing on mitochondria and the gut. *J Diabetes Investig* 6, 600–609.
- Jayaraman P, Sada-Ovalle I, Beladi S, Anderson AC, Dardalhon V, Hotta C, Kuchroo VK, and Behar SM (2010). Tim3 binding to galectin-9 stimulates antimicrobial immunity. *The Journal of experimental medicine* 207, 2343–2354. [PubMed: 20937702]
- Ji YX, Huang Z, Yang X, Wang X, Zhao LP, Wang PX, Zhang XJ, Alves-Bezerra M, Cai L, Zhang P, et al. (2018). The deubiquitinating enzyme cylindromatosis mitigates nonalcoholic steatohepatitis. *Nature medicine* 24, 213–223.
- Jia J, Abudu YP, Claude-Taupin A, Gu Y, Kumar S, Choi SW, Peters R, Mudd MH, Allers L, Salemi M, et al. (2018). Galectins Control mTOR in Response to Endomembrane Damage. *Molecular cell* 70, 120–135 e128. [PubMed: 29625033]
- Johannes L, Jacob R, and Leffler H (2018). Galectins at a glance. *Journal of cell science* 131.
- Jung CH, Jun CB, Ro SH, Kim YM, Otto NM, Cao J, Kundu M, and Kim DH (2009). ULK-Atg13-FIP200 complexes mediate mTOR signaling to the autophagy machinery. *Mol Biol Cell* 20, 1992–2003. [PubMed: 19225151]
- Khaminets A, Heinrich T, Mari M, Grumati P, Huebner AK, Akutsu M, Liebmann L, Stolz A, Nietzsche S, Koch N, et al. (2015). Regulation of endoplasmic reticulum turnover by selective autophagy. *Nature* 522, 354–358. [PubMed: 26040720]
- Kim J, Kim YC, Fang C, Russell RC, Kim JH, Fan W, Liu R, Zhong Q, and Guan KL (2013). Differential regulation of distinct Vps34 complexes by AMPK in nutrient stress and autophagy. *Cell* 152, 290–303. [PubMed: 23332761]
- Kim J, Kundu M, Viollet B, and Guan KL (2011). AMPK and mTOR regulate autophagy through direct phosphorylation of Ulk1. *Nature cell biology* 13, 132–141. [PubMed: 21258367]
- Kim J, Lee HY, Ahn J, Hyun M, Lee I, Min KJ, and You YJ (2016). NHX-5, an Endosomal Na<sup>+</sup>/H<sup>+</sup> Exchanger, Is Associated with Metformin Action. *The Journal of biological chemistry* 291, 18591–18599. [PubMed: 27435670]

- Kimmelman AC, and White E (2017). Autophagy and Tumor Metabolism. *Cell metabolism* 25, 1037–1043. [PubMed: 28467923]
- Kirkin V, McEwan DG, Novak I, and Dikic I (2009). A role for ubiquitin in selective autophagy. *Molecular cell* 34, 259–269. [PubMed: 19450525]
- Kopitz J, Kisen GO, Gordon PB, Bohley P, and Seglen PO (1990). Nonselective autophagy of cytosolic enzymes by isolated rat hepatocytes. *The Journal of cell biology* 111, 941–953. [PubMed: 2391370]
- Lazarou M, Sliter DA, Kane LA, Sarraf SA, Wang C, Burman JL, Sideris DP, Fogel AI, and Youle RJ (2015). The ubiquitin kinase PINK1 recruits autophagy receptors to induce mitophagy. *Nature* 524, 309–314. [PubMed: 26266977]
- Lei CQ, Wu X, Zhong X, Jiang L, Zhong B, and Shu HB (2019). USP19 Inhibits TNF-alpha- and IL-1beta-Triggered NF-kappaB Activation by Deubiquitinating TAK1. *Journal of immunology*.
- Levine B, and Kroemer G (2019). Biological Functions of Autophagy Genes: A Disease Perspective. *Cell* 176, 11–42. [PubMed: 30633901]
- Li L, Liu T, Li Y, Wu C, Luo K, Yin Y, Chen Y, Nowsheen S, Wu J, Lou Z, et al. (2018). The deubiquitinase USP9X promotes tumor cell survival and confers chemoresistance through YAP1 stabilization. *Oncogene* 37, 2422–2431. [PubMed: 29449692]
- Li M, Zhang CS, Zong Y, Feng JW, Ma T, Hu M, Lin Z, Li X, Xie C, Wu Y, et al. (2019). Transient Receptor Potential V Channels Are Essential for Glucose Sensing by Aldolase and AMPK. *Cell metabolism*.
- Li Q, Yan J, Mao AP, Li C, Ran Y, Shu HB, and Wang YY (2011). Tripartite motif 8 (TRIM8) modulates TNFalpha- and IL-1beta-triggered NF-kappaB activation by targeting TAK1 for K63-linked polyubiquitination. *Proceedings of the National Academy of Sciences of the United States of America* 108, 19341–19346. [PubMed: 22084099]
- Lin SC, and Hardie DG (2018). AMPK: Sensing Glucose as well as Cellular Energy Status. *Cell metabolism* 27, 299–313. [PubMed: 29153408]
- Liu CC, Lin YC, Chen YH, Chen CM, Pang LY, Chen HA, Wu PR, Lin MY, Jiang ST, Tsai TF, et al. (2016). Cul3-KLHL20 Ubiquitin Ligase Governs the Turnover of ULK1 and VPS34 Complexes to Control Autophagy Termination. *Molecular cell* 61, 84–97. [PubMed: 26687681]
- Liu W, Jiang Y, Sun J, Geng S, Pan Z, Prinz RA, Wang C, Sun J, Jiao X, and Xu X (2018). Activation of TGF-beta-activated kinase 1 (TAK1) restricts Salmonella Typhimurium growth by inducing AMPK activation and autophagy. *Cell death & disease* 9, 570. [PubMed: 29752434]
- Madeo F, Carmona-Gutierrez D, Hofer SJ, and Kroemer G (2019). Caloric Restriction Mimetics against Age-Associated Disease: Targets, Mechanisms, and Therapeutic Potential. *Cell metabolism* 29, 592–610. [PubMed: 30840912]
- Maejima I, Takahashi A, Omori H, Kimura T, Takabatake Y, Saitoh T, Yamamoto A, Hamasaki M, Noda T, Isaka Y, et al. (2013). Autophagy sequesters damaged lysosomes to control lysosomal biogenesis and kidney injury. *The EMBO journal* 32, 2336–2347. [PubMed: 23921551]
- Manzanillo PS, Shiloh MU, Portnoy DA, and Cox JS (2012). Mycobacterium Tuberculosis Activates the DNA-Dependent Cytosolic Surveillance Pathway within Macrophages. *Cell host & microbe* 11, 469–480. [PubMed: 22607800]
- Marcassa E, Kallinos A, Jardine J, Rusilowicz-Jones EV, Martinez A, Kuehl S, Islinger M, Clague MJ, and Urbe S (2018). Dual role of USP30 in controlling basal pexophagy and mitophagy. *EMBO reports* 19.
- Masters SL, Dunne A, Subramanian SL, Hull RL, Tannahill GM, Sharp FA, Becker C, Franchi L, Yoshihara E, Chen Z, et al. (2010). Activation of the NLRP3 inflammasome by islet amyloid polypeptide provides a mechanism for enhanced IL-1beta in type 2 diabetes. *Nature immunology* 11, 897–904. [PubMed: 20835230]
- Matsushita N, Nishi N, Seki M, Matsumoto R, Kuwabara I, Liu FT, Hata Y, Nakamura T, and Hirashima M (2000). Requirement of divalent galactoside-binding activity of ecalectin/galectin-9 for eosinophil chemoattraction. *The Journal of biological chemistry* 275, 8355–8360. [PubMed: 10722666]

- McCabe MT, Powell DR, Zhou W, and Vertino PM (2010). Homozygous deletion of the STK11/LKB1 locus and the generation of novel fusion transcripts in cervical cancer cells. *Cancer genetics and cytogenetics* 197, 130–141. [PubMed: 20193846]
- Min Y, Lee S, Kim MJ, Chun E, and Lee KY (2017). Ubiquitin-Specific Protease 14 Negatively Regulates Toll-Like Receptor 4-Mediated Signaling and Autophagy Induction by Inhibiting Ubiquitination of TAK1-Binding Protein 2 and Beclin 1. *Frontiers in immunology* 8, 1827. [PubMed: 29326710]
- Mizushima N, Levine B, Cuervo AM, and Klionsky DJ (2008). Autophagy fights disease through cellular self-digestion. *Nature* 451, 1069–1075. [PubMed: 18305538]
- Momcilovic M, Hong SP, and Carlson M (2006). Mammalian TAK1 activates Snf1 protein kinase in yeast and phosphorylates AMP-activated protein kinase in vitro. *The Journal of biological chemistry* 281, 25336–25343. [PubMed: 16835226]
- Nazio F, Strappazon F, Antonioli M, Bielli P, Cianfanelli V, Bordi M, Gretzmeier C, Dengjel J, Piacentini M, Fimia GM, et al. (2013). mTOR inhibits autophagy by controlling ULK1 ubiquitylation, self-association and function through AMBRA1 and TRAF6. *Nature cell biology* 15, 406–416. [PubMed: 23524951]
- Neumann D (2018). Is TAK1 a Direct Upstream Kinase of AMPK? *Int J Mol Sci* 19.
- O'Neill LA, Kishton RJ, and Rathmell J (2016). A guide to immunometabolism for immunologists. *Nat Rev Immunol* 16, 553–565. [PubMed: 27396447]
- Okada M, Matsuzawa A, Yoshimura A, and Ichijo H (2014). The lysosome rupture-activated TAK1-JNK pathway regulates NLRP3 inflammasome activation. *The Journal of biological chemistry* 289, 32926–32936. [PubMed: 25288801]
- Papadopoulos C, Kirchner P, Bug M, Grum D, Koerver L, Schulze N, Poehler R, Dressler A, Fengler S, Arhzaouy K, et al. (2017). VCP/p97 cooperates with YOD1, UBXD1 and PLAA to drive clearance of ruptured lysosomes by autophagy. *The EMBO journal* 36, 135–150. [PubMed: 27753622]
- Parry TL, Melehan JH, Ranek MJ, and Willis MS (2015). Functional Amyloid Signaling via the Inflammasome, Necrosome, and Signalosome: New Therapeutic Targets in Heart Failure. *Front Cardiovasc Med* 2, 25. [PubMed: 26664897]
- Paudel P, Zhang Q, Leung C, Greenberg HC, Guo Y, Chern YH, Dong A, Li Y, Vedadi M, Zhuang Z, et al. (2019). Crystal structure and activity-based labeling reveal the mechanisms for linkage-specific substrate recognition by deubiquitinase USP9X. *Proceedings of the National Academy of Sciences of the United States of America* 116, 7288–7297. [PubMed: 30914461]
- Paz I, Sachse M, Dupont N, Mounier J, Cederfur C, Enninga J, Leffler H, Poirier F, Prevost MC, Lafont F, et al. (2010). Galectin-3, a marker for vacuole lysis by invasive pathogens. *Cell Microbiol* 12, 530–544. [PubMed: 19951367]
- Pineda CT, Ramanathan S, Fon Tacer K, Weon JL, Potts MB, Ou YH, White MA, and Potts PR (2015). Degradation of AMPK by a Cancer-Specific Ubiquitin Ligase. *Cell* 160, 715–728. [PubMed: 25679763]
- Pozhidaeva A, and Bezsonova I (2019). USP7: Structure, substrate specificity, and inhibition. *DNA repair* 76, 30–39. [PubMed: 30807924]
- Rabinowitz JD, and White E (2010). Autophagy and metabolism. *Science* 330, 1344–1348. [PubMed: 21127245]
- Radulovic M, Schink KO, Wenzel EM, Nahse V, Bongiovanni A, Lafont F, and Stenmark H (2018). ESCRT-mediated lysosome repair precedes lysophagy and promotes cell survival. *The EMBO journal* 37.
- Rajani R, Pastor-Soler NM, and Hallows KR (2017). Role of AMP-activated protein kinase in kidney tubular transport, metabolism, and disease. *Curr Opin Nephrol Hypertens* 26, 375–383. [PubMed: 28614117]
- Rambold AS, Cohen S, and Lippincott-Schwartz J (2015). Fatty acid trafficking in starved cells: regulation by lipid droplet lipolysis, autophagy, and mitochondrial fusion dynamics. *Developmental cell* 32, 678–692. [PubMed: 25752962]
- Randow F, and Youle RJ (2014). Self and nonself: how autophagy targets mitochondria and bacteria. *Cell Host Microbe* 15, 403–411. [PubMed: 24721569]

- Razani B, Feng C, Coleman T, Emanuel R, Wen H, Hwang S, Ting JP, Virgin HW, Kastan MB, and Semenkovich CF (2012). Autophagy links inflammasomes to atherosclerotic progression. *Cell metabolism* 15, 534–544. [PubMed: 22440612]
- Reiley WW, Jin W, Lee AJ, Wright A, Wu X, Tewalt EF, Leonard TO, Norbury CC, Fitzpatrick L, Zhang M, et al. (2007). Deubiquitinating enzyme CYLD negatively regulates the ubiquitin-dependent kinase Tak1 and prevents abnormal T cell responses. *The Journal of experimental medicine* 204, 1475–1485. [PubMed: 17548520]
- Rivera JF, Costes S, Gurlo T, Glabe CG, and Butler PC (2014). Autophagy defends pancreatic beta cells from human islet amyloid polypeptide-induced toxicity. *The Journal of clinical investigation* 124, 3489–3500. [PubMed: 25036708]
- Rogov V, Dotsch V, Johansen T, and Kirkin V (2014). Interactions between autophagy receptors and ubiquitin-like proteins form the molecular basis for selective autophagy. *Molecular cell* 53, 167–178. [PubMed: 24462201]
- Rubinsztein DC, Bento CF, and Deretic V (2015). Therapeutic targeting of autophagy in neurodegenerative and infectious diseases. *The Journal of experimental medicine* 212, 979–990. [PubMed: 26101267]
- Sardiello M, Palmieri M, di Ronza A, Medina DL, Valenza M, Gennarino VA, Di Malta C, Donaudo F, Embrione V, Polishchuk RS, et al. (2009). A gene network regulating lysosomal biogenesis and function. *Science* 325, 473–477. [PubMed: 19556463]
- Saxton RA, and Sabatini DM (2017). mTOR Signaling in Growth, Metabolism, and Disease. *Cell* 168, 960–976. [PubMed: 28283069]
- Schroder K, and Tschopp J (2010). The inflammasomes. *Cell* 140, 821–832. [PubMed: 20303873]
- Schwickart M, Huang X, Lill JR, Liu J, Ferrando R, French DM, Maecker H, O'Rourke K, Bazan F, Eastham-Anderson J, et al. (2010). Deubiquitinase USP9X stabilizes MCL1 and promotes tumour cell survival. *Nature* 463, 103–107. [PubMed: 20023629]
- Seglen PO, Gordon PB, and Holen I (1990). Non-selective autophagy. *Semin Cell Biol* 1, 441–448. [PubMed: 2103895]
- Seo AY, Lau PW, Feliciano D, Sengupta P, Gros MAL, Cinquin B, Larabell CA, and Lippincott-Schwartz J (2017). AMPK and vacuole-associated Atg14p orchestrate mu-lipophagy for energy production and long-term survival under glucose starvation. *eLife* 6.
- Settembre C, De Cegli R, Mansueto G, Saha PK, Vetrini F, Visvikis O, Huynh T, Carissimo A, Palmer D, Jurgen Klisch T, et al. (2013). TFEB controls cellular lipid metabolism through a starvation-induced autoregulatory loop. *Nature cell biology* 15, 647–658. [PubMed: 23604321]
- Settembre C, Di Malta C, Polito VA, Garcia Arencibia M, Vetrini F, Erdin S, Erdin SU, Huynh T, Medina D, Colella P, et al. (2011). TFEB links autophagy to lysosomal biogenesis. *Science* 332, 1429–1433. [PubMed: 21617040]
- Singh R, Kaushik S, Wang Y, Xiang Y, Novak I, Komatsu M, Tanaka K, Cuervo AM, and Czaja MJ (2009). Autophagy regulates lipid metabolism. *Nature* 458, 1131–1135. [PubMed: 19339967]
- Singhirunnosorn P, Suzuki S, Kawasaki N, Saiki I, and Sakurai H (2005). Critical roles of threonine 187 phosphorylation in cellular stress-induced rapid and transient activation of transforming growth factor-beta-activated kinase 1 (TAK1) in a signaling complex containing TAK1-binding protein TAB1 and TAB2. *The Journal of biological chemistry* 280, 7359–7368. [PubMed: 15590691]
- Skowrya ML, Schlesinger PH, Naismith TV, and Hanson PI (2018). Triggered recruitment of ESCRT machinery promotes endolysosomal repair. *Science* 360.
- Takaesu G, Kobayashi T, and Yoshimura A (2012). TGFbeta-activated kinase 1 (TAK1)-binding proteins (TAB) 2 and 3 negatively regulate autophagy. *Journal of biochemistry* 151, 157–166. [PubMed: 21976705]
- Thiele DL, and Lipsky PE (1990). Mechanism of L-leucyl-L-leucine methyl ester-mediated killing of cytotoxic lymphocytes: dependence on a lysosomal thiol protease, dipeptidyl peptidase I, that is enriched in these cells. *Proceedings of the National Academy of Sciences of the United States of America* 87, 83–87. [PubMed: 2296607]

- Thurston TL, Wandel MP, von Muhlinen N, Foeglein A, and Randow F (2012). Galectin 8 targets damaged vesicles for autophagy to defend cells against bacterial invasion. *Nature* 482, 414–418. [PubMed: 22246324]
- Wang C, Deng L, Hong M, Akkaraju GR, Inoue J, and Chen ZJ (2001). TAK1 is a ubiquitin-dependent kinase of MKK and IKK. *Nature* 412, 346–351. [PubMed: 11460167]
- Werneburg NW, Guicciardi ME, Bronk SF, Kaufmann SH, and Gores GJ (2007). Tumor necrosis factor-related apoptosis-inducing ligand activates a lysosomal pathway of apoptosis that is regulated by Bcl-2 proteins. *The Journal of biological chemistry* 282, 28960–28970. [PubMed: 17686764]
- Woods A, Johnstone SR, Dickerson K, Leiper FC, Fryer LG, Neumann D, Schlattner U, Wallimann T, Carlson M, and Carling D (2003). LKB1 is the upstream kinase in the AMP-activated protein kinase cascade. *Current biology* : CB 13, 2004–2008. [PubMed: 14614828]
- Wu J, Powell F, Larsen NA, Lai Z, Byth KF, Read J, Gu RF, Roth M, Toader D, Saeh JC, et al. (2013). Mechanism and in vitro pharmacology of TAK1 inhibition by (5Z)-7-Oxozaenol. *ACS chemical biology* 8, 643–650. [PubMed: 23272696]
- Wyant GA, Abu-Remaileh M, Frenkel EM, Laqtom NN, Dharamdasani V, Lewis CA, Chan SH, Heinze I, Ori A, and Sabatini DM (2018). NUFIP1 is a ribosome receptor for starvation-induced ribophagy. *Science* 360, 751–758. [PubMed: 29700228]
- Xie M, Zhang D, Dyck JR, Li Y, Zhang H, Morishima M, Mann DL, Taffet GE, Baldini A, Khoury DS, et al. (2006). A pivotal role for endogenous TGF-beta-activated kinase-1 in the LKB1/AMP-activated protein kinase energy-sensor pathway. *Proceedings of the National Academy of Sciences of the United States of America* 103, 17378–17383. [PubMed: 17085580]
- Yang Z, Xian H, Hu J, Tian S, Qin Y, Wang RF, and Cui J (2015). USP18 negatively regulates NF-kappaB signaling by targeting TAK1 and NEMO for deubiquitination through distinct mechanisms. *Scientific reports* 5, 12738. [PubMed: 26240016]
- Yoshida Y, Yasuda S, Fujita T, Hamasaki M, Murakami A, Kawawaki J, Iwai K, Saeki Y, Yoshimori T, Matsuda N, et al. (2017). Ubiquitination of exposed glycoproteins by SCF(FBXO27) directs damaged lysosomes for autophagy. *Proceedings of the National Academy of Sciences of the United States of America* 114, 8574–8579. [PubMed: 28743755]
- Yu L, McPhee CK, Zheng L, Mardones GA, Rong Y, Peng J, Mi N, Zhao Y, Liu Z, Wan F, et al. (2010). Termination of autophagy and reformation of lysosomes regulated by mTOR. *Nature* 465, 942–946. [PubMed: 20526321]
- Yu Y, Ge N, Xie M, Sun W, Burlingame S, Pass AK, Nuchtern JG, Zhang D, Fu S, Schneider MD, et al. (2008). Phosphorylation of Thr-178 and Thr-184 in the TAK1 T-loop is required for interleukin (IL)-1-mediated optimal NFkappaB and AP-1 activation as well as IL-6 gene expression. *The Journal of biological chemistry* 283, 24497–24505. [PubMed: 18617512]
- Zhang CS, Hawley SA, Zong Y, Li M, Wang Z, Gray A, Ma T, Cui J, Feng JW, Zhu M, et al. (2017). Fructose-1,6-bisphosphate and aldolase mediate glucose sensing by AMPK. *Nature* 548, 112–116. [PubMed: 28723898]
- Zhang CS, Jiang B, Li M, Zhu M, Peng Y, Zhang YL, Wu YQ, Li TY, Liang Y, Lu Z, et al. (2014). The lysosomal v-ATPase-Ragulator complex is a common activator for AMPK and mTORC1, acting as a switch between catabolism and anabolism. *Cell metabolism* 20, 526–540. [PubMed: 25002183]
- Zhang CS, Li M, Ma T, Zong Y, Cui J, Feng JW, Wu YQ, Lin SY, and Lin SC (2016). Metformin Activates AMPK through the Lysosomal Pathway. *Cell metabolism* 24, 521–522. [PubMed: 27732831]
- Zhang Y, Sowers JR, and Ren J (2018). Targeting autophagy in obesity: from pathophysiology to management. *Nat Rev Endocrinol* 14, 356–376. [PubMed: 29686432]
- Zhang YL, Guo H, Zhang CS, Lin SY, Yin Z, Peng Y, Luo H, Shi Y, Lian G, Zhang C, et al. (2013). AMP as a low-energy charge signal autonomously initiates assembly of AXIN-AMPK-LKB1 complex for AMPK activation. *Cell metabolism* 18, 546–555. [PubMed: 24093678]
- Zhou G, Myers R, Li Y, Chen Y, Shen X, Fenyk-Melody J, Wu M, Ventre J, Doebber T, Fujii N, et al. (2001). Role of AMP-activated protein kinase in mechanism of metformin action. *The Journal of clinical investigation* 108, 1167–1174. [PubMed: 11602624]

- Zhu C, Anderson AC, Schubart A, Xiong H, Imitola J, Khoury SJ, Zheng XX, Strom TB, and Kuchroo VK (2005). The Tim-3 ligand galectin-9 negatively regulates T helper type 1 immunity. *Nature immunology* 6, 1245–1252. [PubMed: 16286920]
- Zirin J, Nieuwenhuis J, and Perrimon N (2013). Role of autophagy in glycogen breakdown and its relevance to chloroquine myopathy. *PLoS biology* 11, e1001708. [PubMed: 24265594]

Author Manuscript

Author Manuscript

Author Manuscript

Author Manuscript

**Highlights:**

- Lysosomal damage activates AMPK, autophagy, metabolic and antimicrobial responses
- Galectin 9 transduces damage signal to ubiquitin responses via USP9X and TAK1
- TAK1 controls AMPK in the physiological context of lysosomal permeability changes
- Anti-diabetic drug metformin causes mild lysosomal damage and downstream responses

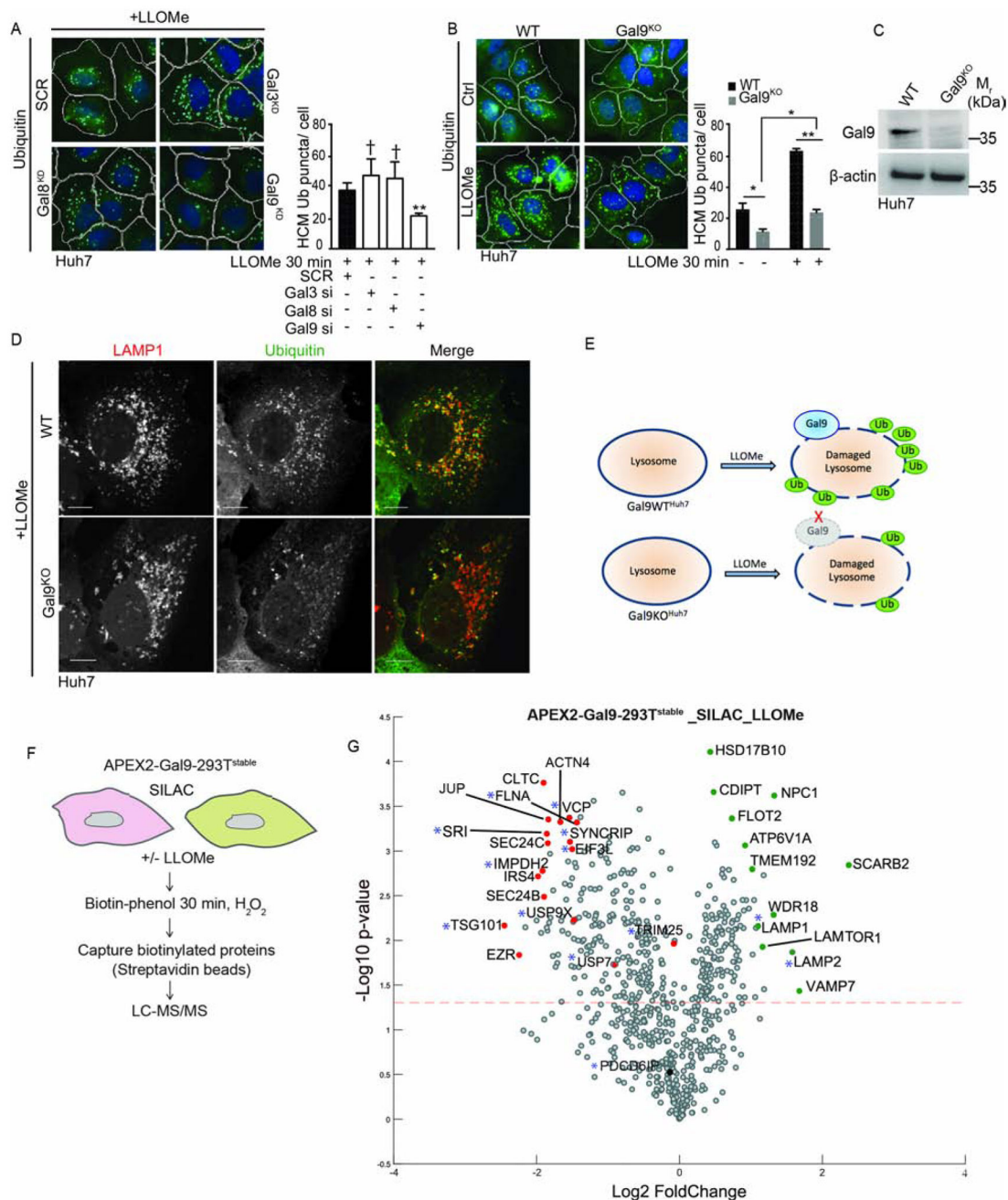


**Figure 1. Gal9 is required for ubiquitination in response to lysosomal damage.**

(A) High content microscopy (HCM) quantification of endogenous ubiquitin (Ub) puncta in Huh7 cells subjected to knockdowns (SCR, scramble siRNA); full medium ± 1mM LLOMe, 30 min. Blue: nuclei, Hoechst 33342; green: anti-Ub FK2 antibody, Alexa-488. White masks, algorithm-defined cell boundaries (primary objects); green masks, computer-identified ubiquitin puncta. HCM data, means ± SEM, n = 3 (each experiment: 500 valid primary objects/cells per well, 5 wells/sample). †p < 0.05 (not significant), \*\*p < 0.01, ANOVA. (B) Ub puncta (FK2) in Gal9<sup>WT</sup>Huh7 and Gal9<sup>KO</sup>Huh7 cells quantified by HCM. Treatment and masks as in A. Ctrl, control untreated cells. HCM data, as in A; \*p < 0.05.

(C) Immunoblot analysis of Gal9 knockouts (Gal9WT<sup>Huh7</sup> and Gal9KO<sup>Huh7</sup>). (D) Confocal microscopy imaging of Ub and LAMP1. Scale bar, 10  $\mu$ M. (E) Summary of the findings in Figures 1 and S1. (F) Schematic, SILAC LC-MS/MS proteomics using APEX2-Gal9-293T<sup>stable</sup> (see STAR Methods). (G) Volcano plot, protein proximity biotinylation dynamics with APEX2-Gal9 (from SILAC LC-MS/MS data in Table S1, Tabs 2 and 3; 3 independent biological experiments) upon lysosomal damage (1mM LLOMe, 1 h). Red and green, Gal9 partners of interest with reduced and increased abundance after lysosomal damage (Log2 fold change, Log2 of LLOMe: control ratio; dashed line,  $-\text{Log}_{10}$  statistical significance cutoff ( $p < 0.05$ )). Asterisks, proteins identified by LC-MS/MS after lysosomal damage with GPN (see Figure 3A). See also Figure S1.

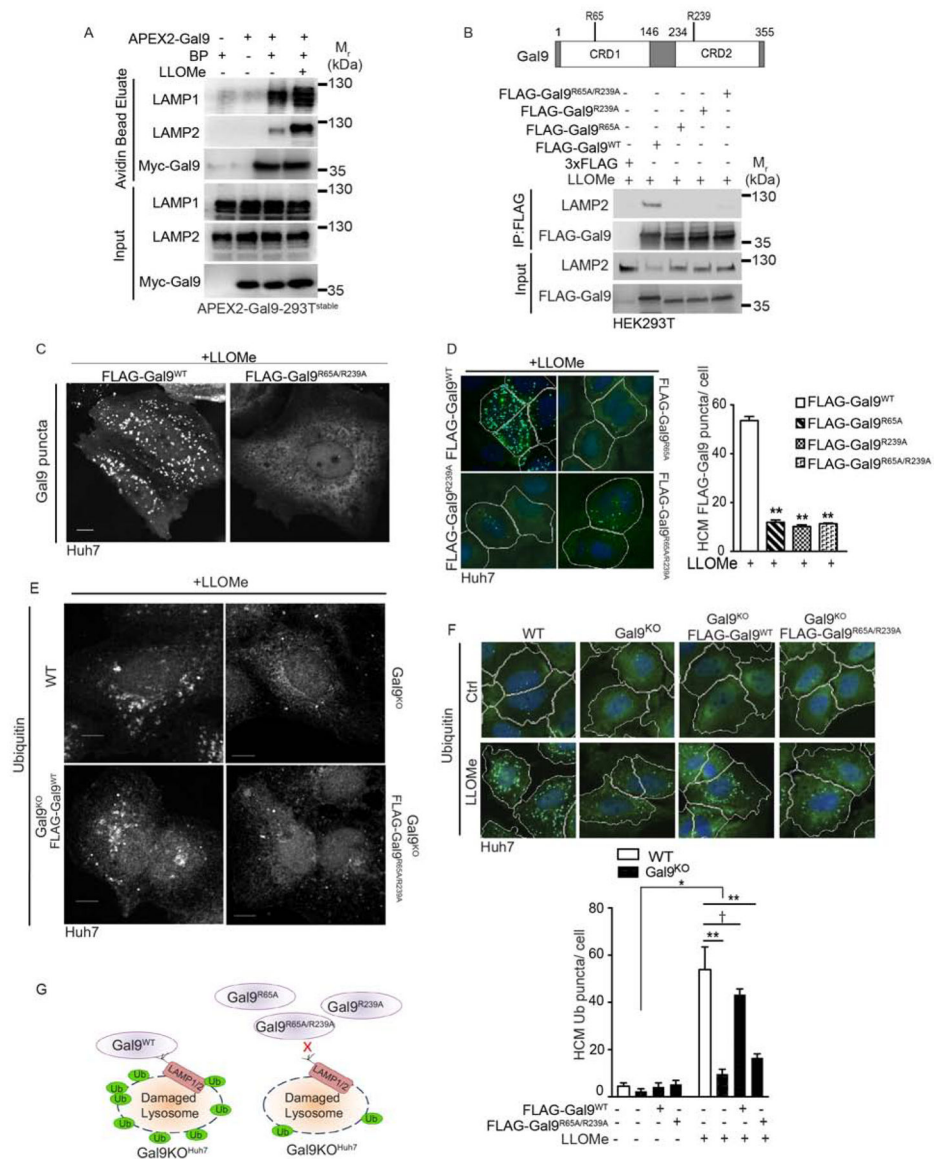


**Figure 2. Gal9 recruitment to damaged lysosomes regulates ubiquitination response**

(A) BioWeB analysis (see STAR methods) of HEK293T cells expressing (+) APEX2-myc-Gal9 (APEX2-Gal9-293T<sup>stable</sup> cells) or not (-), incubated with 1 mM LLOMe for 30 min, with or without biotin-phenol (BP), and pulsed with H<sub>2</sub>O<sub>2</sub>. Biotinylated proteins were affinity-enriched (eluate) on streptavidin beads and analyzed by immunoblotting. (B) Co-immunoprecipitation (Co-IP) analysis of LAMP2-Gal9 interactions. HEK293T cells expressing FLAG-tagged Gal9 or glycan-recognition mutants of Gal9 (R65A, R239A, or combined R65A/R239A) were treated with 1 mM LLOMe for 30 min. (C) Confocal microscopy of Gal9 puncta in Huh7 cells transfected with FLAG-Gal9<sup>WT</sup> or double mutant FLAG-Gal9<sup>R65A/R239A</sup> treated 30 min with 1mM LLOMe. Cells were immunostained for FLAG. Scale bar, 10  $\mu$ M. (D) HCM quantification of FLAG-Gal9 puncta in Huh7 cells transfected with FLAG-Gal9<sup>WT</sup> or mutants. HCM, blue: nuclei, Hoechst 33342; green: anti-FLAG, Alexa-488). White masks, algorithm-defined cell boundaries; green masks,

computer-identified FLAG-Gal9 puncta. (E) Confocal visualization of endogenous Ub puncta in Gal9WT<sup>Huh7</sup> and Gal9KO<sup>Huh7</sup> cells complemented with FLAG-Gal9<sup>WT</sup> or FLAG-Gal9<sup>R65A/R239A</sup>. Treatment as in D. Scale bar, 10  $\mu$ M. (F) Endogenous Ub puncta quantified by HCM. Cells treatment as in (E). Ctrl, untreated cells. Masks as in D, except green masks, Ub puncta. (G) Summary of findings in Figures 2 and S2. HCM data, means  $\pm$  SEM; n = 3 (each experiment: 500 valid primary objects/cells per well, 5 wells/sample). <sup>†</sup>p > 0.05 (not significant), \*p < 0.05, \*\*p < 0.01, ANOVA. See also Figure S2.

Author Manuscript

Author Manuscript

Author Manuscript

Author Manuscript

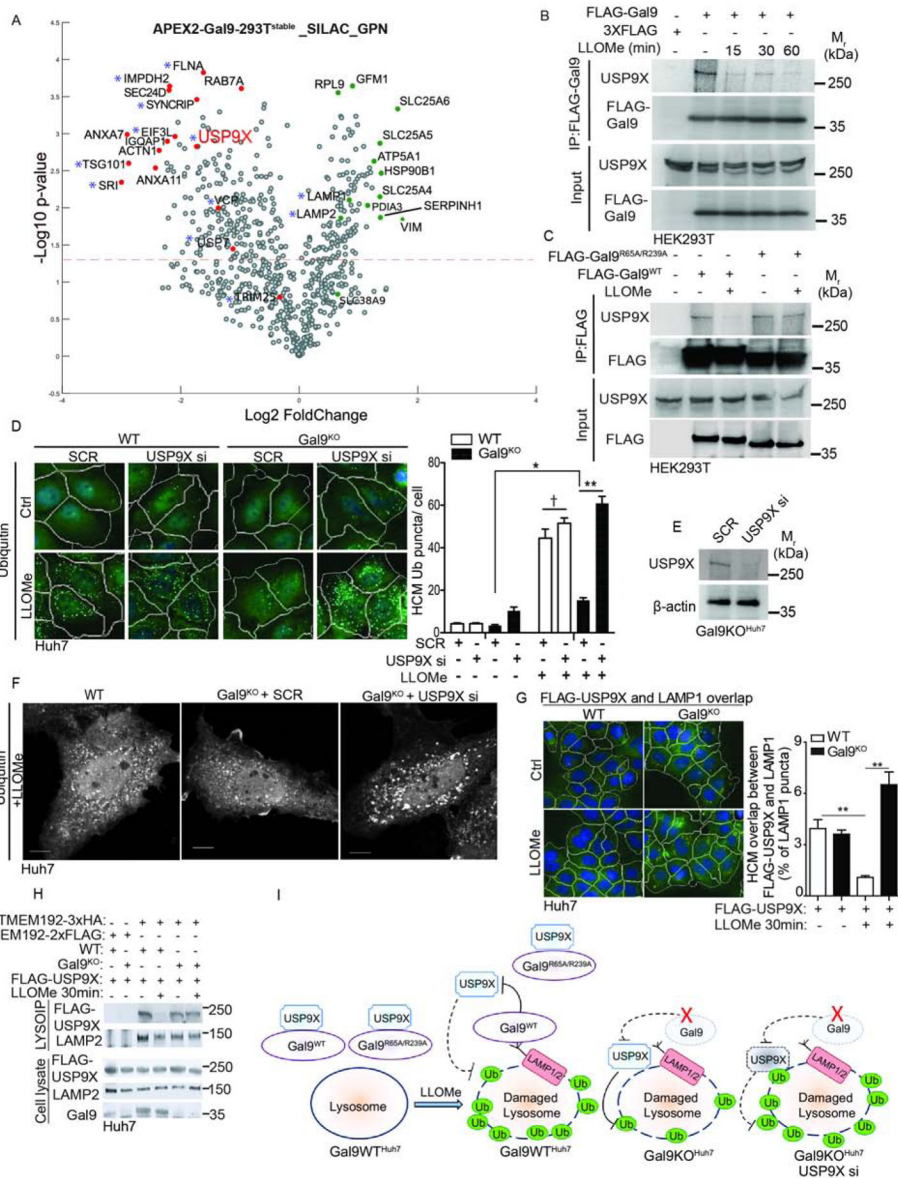


**Figure 3. Deubiquitinating enzyme USP9X is a Gal9 interactor and plays a role in ubiquitin response to lysosomal damage**  
 (A) Volcano plot, protein proximity biotinylation dynamics in APEX2-Gal9–293<sup>stable</sup> cells from SILAC LC-MS/MS data in Table S1, Tabs 2 and 4 (3 independent biological experiments), lysosomal damage (100 μM GPN, 1 h) vs control. Red and green, Gal9 partners of interest with reduced and increased abundance after lysosomal damage (Log<sub>2</sub> fold change, GPN: control ratio; dashed line, –Log<sub>10</sub> statistical significance cutoff (p 0.05). Asterisks, overlaps with proteins of interest in Figure 1G. (B) Co-IP analysis of endogenous USP9X in HEK293T cells expressing FLAG-Gal9 and treated with 1 mM LLOMe. (C) Co-IP analysis of FLAG-Gal9<sup>WT</sup> or FLAG-Gal9<sup>R65A/R239A</sup> and endogenous USP9X 1 mM LLOMe, 30 min. (D) HCM quantification of endogenous Ub puncta in Gal9<sup>WT</sup><sup>Huh7</sup> and Gal9<sup>KO</sup><sup>Huh7</sup> cells transfected with USP9X or scramble (SCR) siRNA and treated with 1mM LLOMe 30 min, (blue: nuclei, Hoechst 33342; green: anti-FK2 Ub

antibody, Alexa-488). (E) WB analysis of USP9X knockdown in Gal9KO<sup>Huh7</sup> cells. (F) Confocal microscopy of endogenous Ub puncta. Scale bar, 10  $\mu$ M. (G) HCM quantification of FLAG-USP9X and LAMP1 overlaps in Gal9WT<sup>Huh7</sup> and Gal9KO<sup>Huh7</sup> cells; 1mM LLOMe treatment. White masks, algorithm-defined cell; Yellow masks, computer-identified overlap of FLAG-USP9X and LAMP1. (H) Lysosomes purified by LysoIP from Gal9WT<sup>Huh7</sup> and Gal9KO<sup>Huh7</sup> cells transfected with FLAG-USP9X. 1mM LLOMe. (I) Schematic summary of the findings in Figures 3 and S3. HCM data, means  $\pm$  SEM; n = 3 (each experiment: 500 valid primary objects/cells per well, 5 wells/sample). †p < 0.05 (not significant), \*p < 0.05, \*\*p < 0.01, ANOVA.

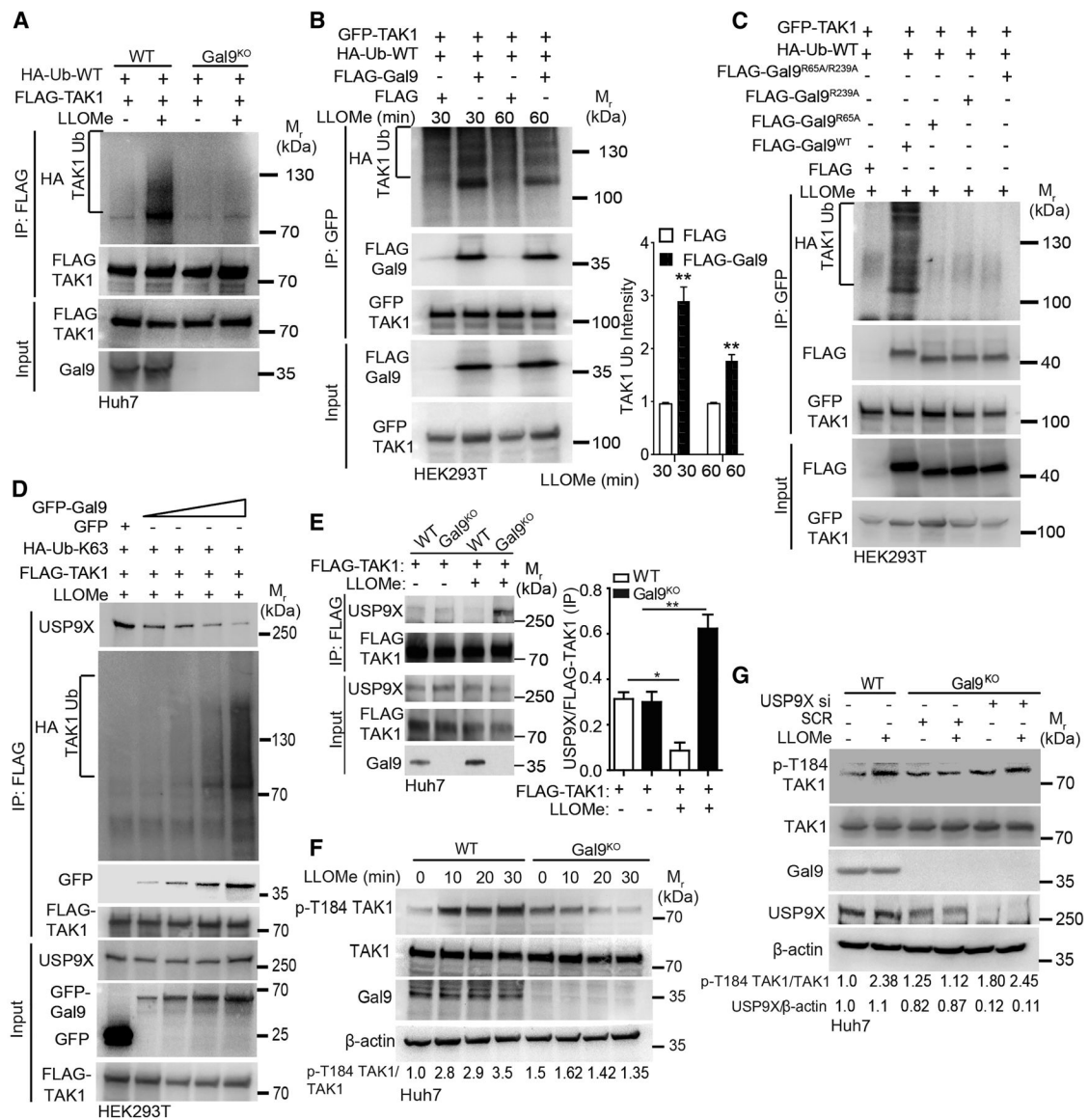


**Figure 4. Ubiquitin and USP9X in response to lysosomal damage converge upon TAK1, an upstream regulator of AMPK**

(A) TAK1 ubiquitination analysis in Gal9<sup>WT</sup><sup>Huh7</sup> and Gal9<sup>KO</sup><sup>Huh7</sup> cells transfected with FLAG-TAK1 and HA-Ub-WT and treated with 1mM LLOMe for 30min. IP, anti-FLAG antibody; immunoblot for Ub, anti-HA antibody. (B) TAK1 ubiquitination analysis in HEK293T cells transfected with GFP-TAK1, HA-Ub-WT and FLAG or FLAG-Gal9 and treated with 1mM LLOMe for 30min or 60min. (C) TAK1 ubiquitination analysis in HEK293T cells transfected with GFP-TAK1, HA-Ub-WT and FLAG or FLAG-Gal9<sup>WT</sup>/FLAG-Gal9<sup>R65A</sup>/FLAG-Gal9<sup>R239A</sup>/FLAG-Gal9<sup>R65A/R239A</sup> and treated with 1mM LLOMe for 30min. (D) Analyses of FLAG-TAK1-USP9X(endogenous) interactions and analysis of TAK1 K63 ubiquitination. HEK293T cells were transfected with FLAG-TAK1, HA-Ub-K63 and GFP or GFP-Gal9 in increasing amounts (0.5, 1, 2.5 and 5 $\mu$ g) and treated with 1mM LLOMe for 30min. (E) Co-IP analysis of interactions between FLAG-TAK1 and endogenous USP9X in Gal9<sup>WT</sup><sup>Huh7</sup> and Gal9<sup>KO</sup><sup>Huh7</sup>. Cells transfected with FLAG-TAK1

were treated with 1mM LLOMe for 30min. (F) WB analysis of phospho-TAK1 in Gal9WT<sup>Huh7</sup> and Gal9KO<sup>Huh7</sup> cells treated with 1mM LLOMe. (G) WB analysis of phospho-TAK1 in Gal9WT<sup>Huh7</sup> and Gal9KO<sup>Huh7</sup> cells with knockdowns as indicated; 1mM LLOMe for 30 min. Data, means  $\pm$  SEM; immunoblots, n = 3; \*p < 0.05, \*\*p < 0.01, ANOVA.

Author Manuscript

Author Manuscript

Author Manuscript

Author Manuscript



to Gal9 knockdown in response to the treatment with 10 $\mu$ g/mL TRAIL for 1h. White masks, as in G; green masks, computer-identified ubiquitin puncta. (I-J) Analysis of the activation of AMPK in Huh7 cells subjected to knockdowns treated with 1mM LLOMe for 30min (I) or 2h (J). AMPK activity was monitored by immunoblotting analysis of AMPK $\alpha$  (p-T172) and acetyl-CoA carboxylase (ACC, p-S79) phosphorylation. Cells transfected with scrambled siRNA were as control (SCR). (K) AMP/ATP ratio in Huh7 cells in response to 1mM LLOMe treatment and duration. Data, means  $\pm$  SEM; HCM n = 3 (each experiment: 500 valid primary objects/cells per well, 5 wells/sample). AMP/ATP ratios, n=3. Significance: \*p < 0.05, \*\*p < 0.01, ANOVA.

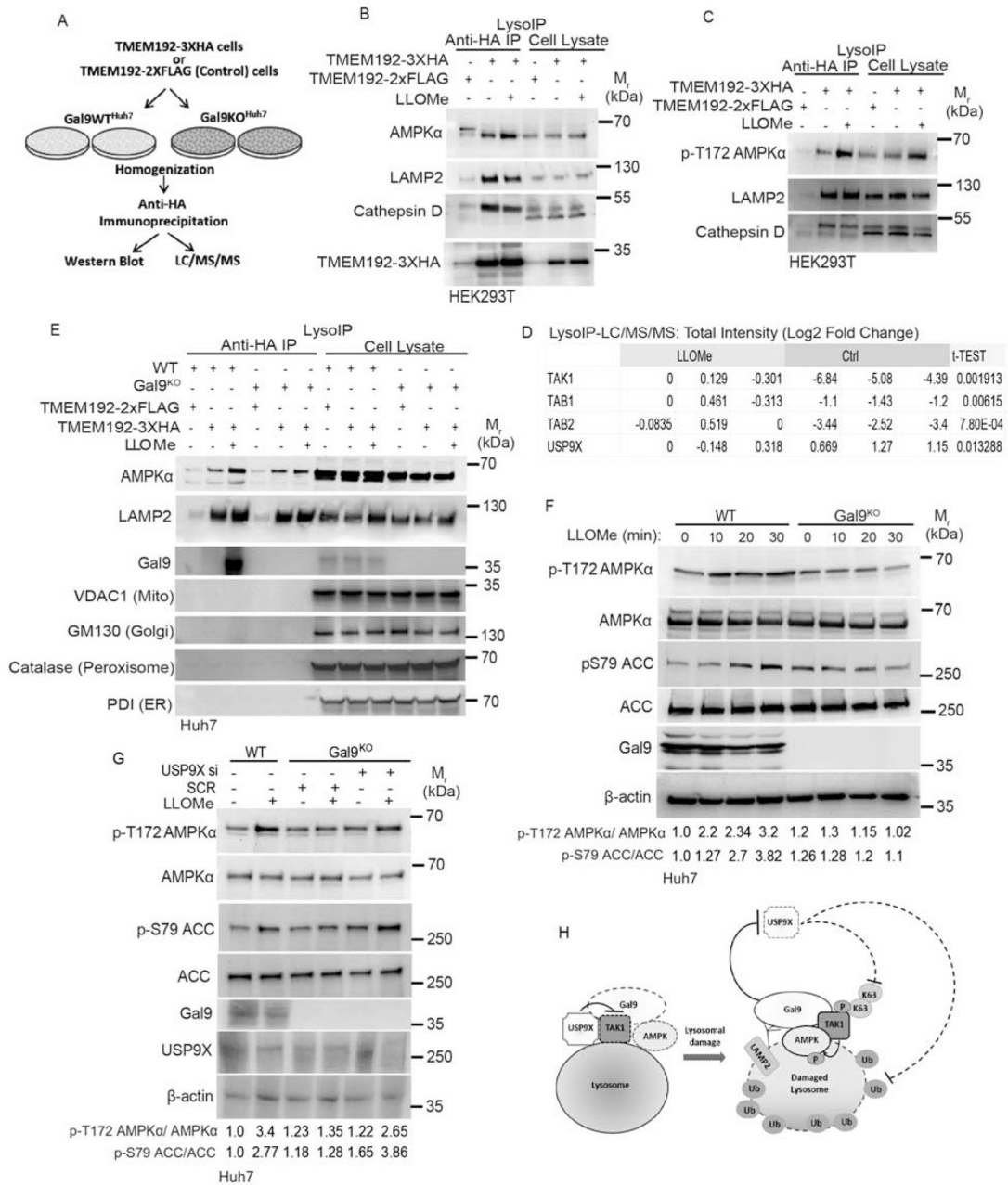


**Figure 6. Activated AMPK translocate to lysosomes in a Gal9-dependent manner**

(A-C) Immunoblot analysis for indicated proteins in cell lysates or purified lysosomes (by LysoIP) from HEK293T cells subjected to 1mM LLOMe treatment for 30min. (D) Summary of LysoIP LC-MS/MS proteomic DIA analysis from HEK293T cells (see STAR methods, and Table S1, Tabs 7–9). (E) LysoIP analysis (see schematic in A) of indicated proteins in Gal9WT<sup>Huh7</sup> and Gal9KO<sup>Huh7</sup> cells subjected to 1mM LLOMe treatment for 30min. (F) WB analysis of AMPK activation in Gal9WT<sup>Huh7</sup> and Gal9KO<sup>Huh7</sup> cells treated with 1mM LLOMe. (G) WB analysis as in F without (SCR) or with USP9X knockdown (H) Overall schematic summary.

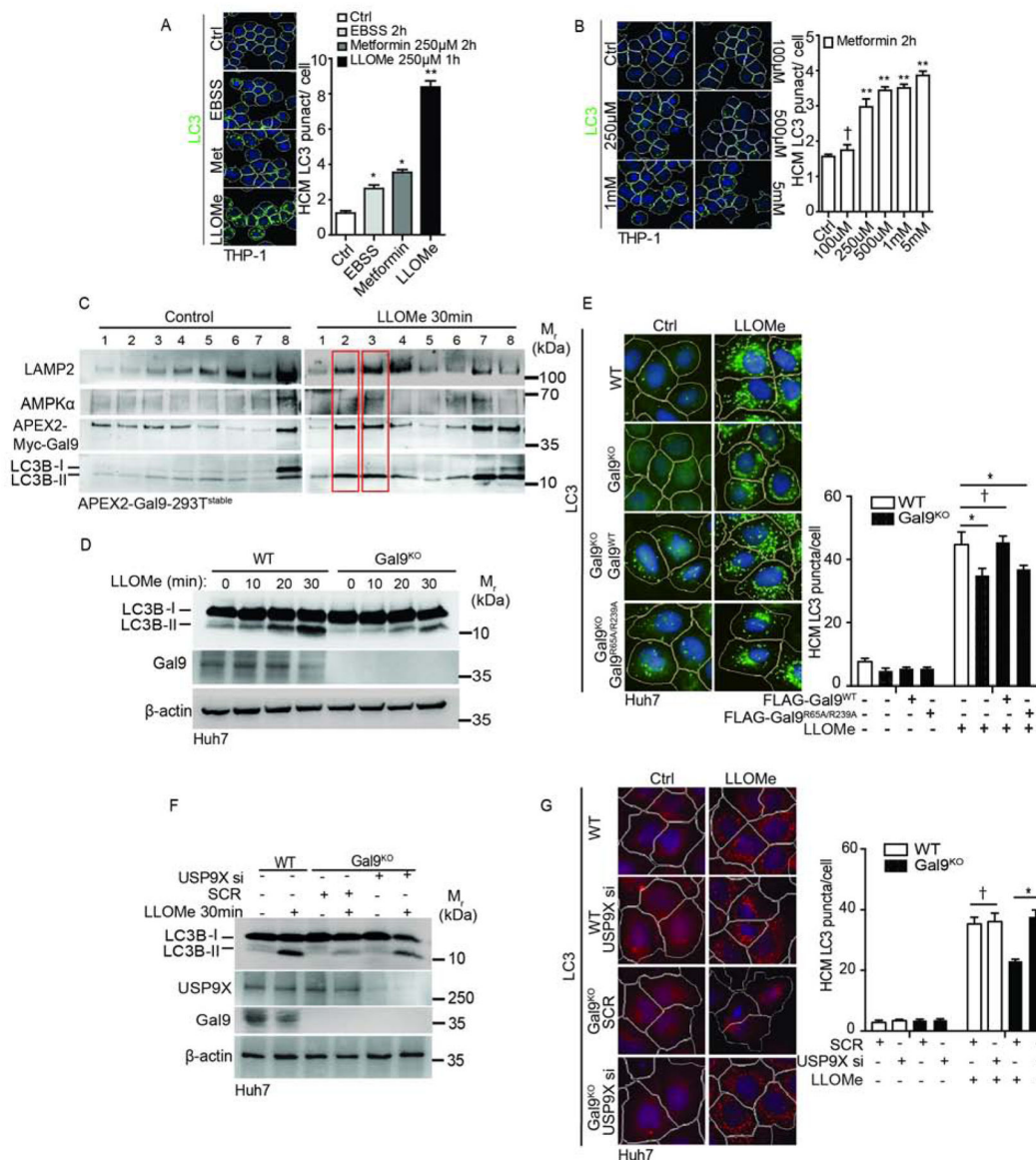


**Figure 7. Gal9 and USP9X regulate autophagy response to lysosomal damage**

(A) THP-1 cells were starved in EBSS or treated in full medium with 250μM metformin for 2h or 250μM LLOMe for 1h, and the mean area/cell of LC3 puncta was determined by HCM. White masks, algorithm-defined cell boundaries; green masks, computer-identified LC3 puncta. (B) THP-1 cells were treated with escalating doses of metformin and analyzed as in A. (C) Proteins in membrane fractions (OptiPrep gradients; 1–8 fractions, light to heavy). Red boxes, shift of proteins to lighter fractions in LLOMe treated cells. (D) LC3-II conversion analysis (WB) in Gal9<sup>WT</sup><sup>Huh7</sup> and Gal9<sup>KO</sup><sup>Huh7</sup> cells treated with 1mM LLOMe. (E) HCM quantification of LC3 puncta. Cells transfected with Gal9<sup>WT</sup> or its mutant Gal9<sup>R65A/R239A</sup>, were treated with LLOMe for 30 min (F) LC3-II analysis as in D. Gal9<sup>KO</sup><sup>Huh7</sup> were transfected with siRNA treated and processed as in D. (G) HCM quantification of LC3 puncta as in (E) with USP9X KD. White masks, algorithm defined cell boundaries; red masks, computer-identified LC3 puncta. HCM data, means ± SEM; n

3 (each experiment: 500 valid primary objects/cells per well, 5 wells/sample). †p 0.05 (not significant), \*p < 0.05, \*\*p < 0.01, ANOVA.

Author Manuscript

Author Manuscript

Author Manuscript

Author Manuscript

## KEY RESOURCES TABLE

REAGENT or RESOURCE	SOURCE	IDENTIFIER
Antibodies		
Rabbit Anti-GFP	Abcam	ab290
Rabbit Anti-GFP(6AT316)	Abcam	ab38689
Rabbit Anti-mCherry	Abcam	ab183628
Rabbit Anti-VDAC1/Porin	Abcam	ab15895
Mouse Anti-GM130	Abcam	ab1299
Mouse Anti-P4HB(PDI) (RL90)	Abcam	ab2792
Rabbit Anti-Galectin 9	Abcam	ab69630
Rabbit Anti-USP9X	Abcam	ab19879
Rabbit Anti-LKB1	Abcam	ab61122
Rabbit Anti-CaMKK2	Abcam	ab96531
Rabbit Cathepsin D	Abcam	ab6313
Rabbit Anti-LC3	MBL International	PM036
Rabbit Anti-ATG16L1	MBL International	PM040
Mouse Anti-Galectin 3	BioLegend	#125402
Rabbit Anti-p-AMPK $\alpha$ (T172)	Cell Signaling Technology	#2535
Rabbit Anti-AMPK $\alpha$	Cell Signaling Technology	#2532
Rabbit Anti-p-ACC (S79)	Cell Signaling Technology	#11818
Rabbit Anti-ACC	Cell Signaling Technology	#3662
Rabbit Anti-p-ULK1 (S555)	Cell Signaling Technology	#5869
Rabbit Anti-ULK1(D9D7)	Cell Signaling Technology	#6439
Rabbit Anti-p-TAK1 (T184/187) (90C7)	Cell Signaling Technology	#4508
Rabbit Anti-TAK1	Cell Signaling Technology	#5206
Rabbit Anti-HA	Cell Signaling Technology	#3724S
Rabbit ATG13 (E1Y9V)	Cell Signaling Technology	#13468
Rabbit LAMP1 (D2D11)	Cell Signaling Technology	#9091
Rabbit AXIN (C76H11)	Cell Signaling Technology	#2087
Mouse Anti-FLAG M2	Sigma Aldrich	F1804
Mouse LAMP2	DSHB of University of Iowa	H4B4
Mouse Anti-Ubiquitin (FK2)	Millipore	04-263
Mouse Anti-ALIX	BioLegend	#634502
Rabbit Anti-Catalase	Calbiochem	219010
Goat Anti-Galectin 9	R & D	AF2045
Clean-Blot IP Detection Kit (HRP)	ThermoFisher	21232
Alexa Fluor 488 secondary antibody	ThermoFisher	A-11029
Alexa Fluor 568 secondary antibody	ThermoFisher	A-11036
Mouse Anti-c-Myc	Santa Cruz Biotechnology	sc-40

REAGENT or RESOURCE	SOURCE	IDENTIFIER
Rabbit beta-Actin (C4)	Santa Cruz Biotechnology	sc-47778
Rabbit Galectin 8(H-80)	Santa Cruz Biotechnology	sc-28254
Goat anti-rabbit IgG-HRP secondary antibody	Santa Cruz Biotechnology	sc-2004
Goat anti-mouse IgG-HRP secondary antibody	Santa Cruz Biotechnology	sc-2005
<b>Bacterial and Virus Strains</b>		
NEB 5-alpha Competent <i>E.coli</i> (High Efficiency)	New England Biolabs	C2987
One Shot Mach1 Phage-Resistant Competent <i>E.coli</i>	ThermoFisher	C862003
<i>Mycobacterium tuberculosis</i> Erdman	Manzanillo et al., 2012	N/A
<b>Biological Samples</b>		
Human peripheral blood monocyte cells	Consented human volunteers, University of New Mexico Clinical and Translational Science Center	N/A
<b>Chemicals, Peptides, and Recombinant Proteins</b>		
Leu-Leu-methyl ester hydrobromide (LLOMe)	Sigma Aldrich	L7393
Gly-Phe-beta-Naphthylamide (GPN)	Cayman Chemicals	21438-66-4
Biotinyl tyramide (biotin-phenol)	AdipoGen LIFE SCIENCES	CDX-B0270-M100
TRAIL/APO 2 ligand	Neuromics	PR27058
A23187	Sigma Aldrich	C7522
Ionomycin	InvivoGen	N/A
Oligomycin A	Sigma Aldrich	75351
sodium ascorbate	Sigma Aldrich	A7631
sodium azide	Sigma Aldrich	S2002
Trolox	Sigma Aldrich	238813
Tetracycline hydrochloride	Sigma Aldrich	T3383
Puromycin dihydrochloride	Sigma Aldrich	P9620
TAK1 inhibitor (5Z-oxozeanol)	Sigma Aldrich	O9890
Silica crystal	US Silica	MIN-U-SIL-15
mouse macrophage colony stimulating factor (mM-CSF)	Cell Signaling Technology	5228
Hygromycin B (50mg/mL)	ThermoFisher	10687010
LysoTracker Red DND-99	ThermoFisher	L7528
Hoechst 33342	ThermoFisher	H3570
Prolong Gold Antifade Mountant with DAPI	ThermoFisher	P36931
LR Clonase II Plus Enzyme Mix	ThermoFisher	11791100
BP Clonase II Plus Enzyme Mix	ThermoFisher	11789100
<b>Critical Commercial Assays</b>		
ProFection Mammalian Transfection System	Promega	E1200
Amaya Cell Line Nucleofector Kit R	Lonza	VCA-1001
QuickChange Lightning Muti Site-Directed Mutagenesis Kit	Agilent	210515
Magic Red Cathepsin-B Assay	ImmunoChemistry	#938
ATP/ADP/AMP Assay Kit	Biomedical Research Service & Clinical Application	A-125

REAGENT or RESOURCE	SOURCE	IDENTIFIER
Lipofectamine RNAiMAX Transfection Reagent	ThermoFisher	13778030
Lipofectamine 2000 Transfection Reagent	ThermoFisher	12566014
<b>Deposited Data</b>		
Raw MS data	<a href="http://www.proteomexchange.org">http://www.proteomexchange.org</a>	ProteomeXchange: PXD015779
Original imaging data (microscopy and western blots)	This paper; Mendeley Data	<a href="http://dx.doi.org/10.17632/4gb6s7mhh7.1">http://dx.doi.org/10.17632/4gb6s7mhh7.1</a>
<b>Experimental Models: Cell Lines</b>		
HeLa Flp-In-Gal9 <sup>Tet-ON</sup>	This study	N/A
APEX2-Gal9-293T <sup>stable</sup>	This study	N/A
HEK293T TMEM192-3XHA	This study	N/A
HEK293T TMEM192-2XFLAG	This study	N/A
Gal9WT <sup>Huh7</sup> TMEM192-2XFLAG	This study	N/A
Gal9WT <sup>Huh7</sup> TMEM192-3XHA	This study	N/A
Gal9KO <sup>Huh7</sup> TMEM192-2XFLAG	This study	N/A
Gal9KO <sup>Huh7</sup> TMEM192-3XHA	This study	N/A
Gal9KO <sup>Huh7</sup>	This study	N/A
TAB2 KO MEFs	Shizuo Akira, Osaka University	N/A
<b>Experimental Models: Organisms/Strains</b>		
CX3CR1 AMPK $\alpha$ 1 <sup>fl/fl</sup> /AMPK $\alpha$ 2 <sup>fl/fl</sup> mice Genotyping service provided by Transnetyx	Kenneth R. Hallows, USC	N/A
<b>Oligonucleotides</b>		
Gal9 <sup>R65A</sup> -mutant oligonucleotide sense 5'-ccttcacactcaaccctcgcttgaagatggagggt-3'	Integrated DNA Technologies	N/A
Gal9 <sup>R65A</sup> -mutant oligonucleotide anti-sense 5'-accctccatctcaaacgcagggtgaagtggaagg-3'	Integrated DNA Technologies	N/A
Gal9 <sup>R239A</sup> -mutant oligonucleotide sense 5'-ccttcacactgaaccccgcttggatgagaatgctg-3'	Integrated DNA Technologies	N/A
Gal9 <sup>R239A</sup> -mutant oligonucleotide anti-sense 5'-cagcattctcatcaaaagcgggtcaggtggaagg-3'	Integrated DNA Technologies	N/A
Gal9 CRD1 oligonucleotide sense 5'-ggggacaagttgtacaaaaagcaggcttcgcttcagcgggtcccaggctc-3'	Integrated DNA Technologies	N/A
Gal9 CRD1 oligonucleotide anti-sense 5'-ggggaccactttgtacaagaaagctgggtcctagctgatgagacagctgc-3'	Integrated DNA N/A Technologies	N/A
Gal9 CRD2 oligonucleotide sense 5'- ggggacaagttgtacaaaaagcaggcttcgggctgtaccatccaagtccatc-3'	Integrated DNA Technologies	N/A
Gal9 CRD2 oligonucleotide anti-sense 5'-ggggaccactttgtacaagaaagctgggtcctatgtctgcacatgggtcagc-3'	Integrated DNA Technologies	N/A
SiGENOME human USP9X siRNA (SMARTpool)	Dharmacon	M-004233-02-0005
<b>Recombinant DNA</b>		
pRK5-HA-Ubiquitin-WT	Lim et al., 2005	Addgene #17608
pRK5-HA-Ubiquitin-K48	Lim et al., 2005	Addgene #17605
pRK5-HA-Ubiquitin-K63	Lim et al., 2005	Addgene #17606
pLJC5-TMEM192-3XHA	Abu-Remaileh et al., 2017	Addgene #102930

REAGENT or RESOURCE	SOURCE	IDENTIFIER
pLJC5-TMEM192-2XFLAG	Abu-Remaileh et al., 2017	Addgene #102929
pCMV-VSV-G	Stewart et al., 2003	Addgene #8454
psPAX2	Trono lab	Addgene #12260
pENTR223-USP9X	DNASU	MmCD00297218
pDEST-mCherry-Gal9	This study	N/A
pDEST-FLAG-Gal9 <sup>R65A</sup>	This study	N/A
pDEST-FLAG-Gal9 <sup>R239A</sup>	This study	N/A
pDEST-FLAG-Gal9 <sup>R65A/R239A</sup>	This study	N/A
pDEST-GFP-LKB1	This study	N/A
pDEST-FLAG-USP9X	This study	N/A
pDEST-SLC22A1-GFP	This study	N/A
pDEST-SLC22A1-FLAG	This study	N/A
pDEST-Gal9 CRD1 (1–146)	Jia et al., 2018	N/A
pDEST-Gal9 CRD2 (234–355)	Jia et al., 2018	N/A
pJiaDEST-APEX2-Gal9	Jia et al., 2018	N/A
pDEST-GFP-Gal8	Jia et al., 2018	N/A
pDEST-GFP-Gal9	Jia et al., 2018	N/A
pDEST-FLAG-Gal9	Jia et al., 2018	N/A
pDEST-GFP-TAK1	Jia et al., 2018	N/A
pDEST-FLAG-TAK1	Jia et al., 2018	N/A
pDEST-Flp-In-APEX2-AMPK $\alpha$ 1	This study	N/A
<b>Software and Algorithms</b>		
iDEV software	ThermoFisher	N/A
VANTED software	Junker et al., 2006	<a href="http://vanted.ipk-gatersleben.de">http://vanted.ipk-gatersleben.de</a>
AIM software	Carl Zeiss	<a href="https://www.zeiss.com/microscopy/us/downloads.html">https://www.zeiss.com/microscopy/us/downloads.html</a>
Scaffold software	Proteome Software Inc	<a href="http://www.proteomesoftware.com/products/free-trial/">http://www.proteomesoftware.com/products/free-trial/</a>
MATLAB software	MathWorks	<a href="https://www.mathworks.com/campaigns/products/trials.html">https://www.mathworks.com/campaigns/products/trials.html</a>
<b>Other</b>		
RIPA Lysis Buffer	ThermoFisher	89900
NP40 Cell Lysis Buffer	ThermoFisher	FNN0021
Protease Inhibitor Cocktail Tablets	Roche	11697498001
PMSF	Sigma Aldrich	93482
Anti-HA Magnetic Beads	ThermoFisher	88836
Dynabeads Protein G	ThermoFisher	10003D
Streptavidin Magnetic Beads	ThermoFisher	88816
DMEM, no glucose	ThermoFisher	11966025